Master Thesis

Molecular junctions based on an electrofluorochromic polymer

Laboratory:

Photophysique et photochimie supramoléculaires et macromoléculaires (PPSM)

ENS-Paris-Saclay

Author:

Jennifer Calderón Mora

Supervised by :

Pr. Fabien Miomandre, Director of PPSM

Dr. Vitor Brasiliense, Researcher at PPSM

July 2023

This page was intentionally left blank

Table of Contents

Abstract

Electrofluorochromic (EFC) conjugated polymers are characteristic for their luminescence that can be reversibly controlled by their redox state, which makes them promising materials for applications in molecular electronics, like displays and sensor devices. The coupling of these polymers with plasmonic surfaces allows for the multimodal control of luminescence, opening the possibility of both electrochemically- and plasmonically- controllable devices. The aim of this project is to investigate how the conducting properties of a conjugated polymer can be tuned by plasmon excitation, using SECM, fluorescence and optical microscopies as sensitive detection techniques.

The EFC system used in this study is the dyad monomer RDCZ composed of a fluorophore (rhodamine) and an electropolymerizable unit (carbazole). The polymerization of this compound was explored both through electrochemical and photophysical strategies, producing a conjugated polymer (PolyRDCZ) that shows promising electrofluorochromic properties and capacity for micro/nanofabrication of complex structures. The potential induced modulation of absorbance and emission spectra was studied through spectroelectrochemical kinetic experiments.

In the final stage of this project, a molecular junction was constructed using a novel photo/electrochemical approach to polymerize PolyRDCZ between a Pt ultramicroelectrode and a plasmonic substrate. The coupled electrical and fluorescence response of the junction was detected under the stimuli of a plasmonic excitation.

Key words: Photophysics, Electrochemistry, Fluorescence microscopy, Scanning ElectroChemical Microscopy (SECM), Electrofluorochromism

Resumé

Les polymères conjugués électrofluorochromiques (EFC) sont caractérisés par leur luminescence, qui peut être contrôlée de façon réversible en modulant leur état redox, ce qui en fait des matériaux prometteurs pour des applications en électronique moléculaire pour la réalisation d'écrans ou de capteurs. Le couplage de ces polymères avec des surfaces plasmoniques permet le contrôle multimodal de la luminescence, ouvrant voie à des dispositifs électrochimiques et plasmoniques contrôlables. L'objectif de ce projet est d'étudier comment les propriétés conductrices d'un polymère conjugué peuvent être contrôlées sous excitation plasmonique, en utilisant des techniques de SECM et microcopies optiques comme techniques de détection sensibles.

Le système EFC utilisé dans cette étude est le monomère de dyades (RDCZ), composé d'un fluorophore (rhodamine) et d'une unité électropolymérisable (carbazole). Nous avons exploré des stratégies électrochimiques et photophysiques pour contrôler la polymérisation de ce composé, produisant un polymère conjugué (PolyRDCZ) qui montre des propriétés électrofluorochromiques prometteuses et capacité de micro/nanofabrication de structures complexes. La modulation du potentiel induit des changements sur les spectres d'absorbance et d'émission des polymères conjugués qui sont étudiés par des expériences cinétiques spectroélectrochimiques.

Dans la dernière étape de ce projet, une jonction moléculaire a été construite en utilisant une nouvelle approche photo/électrochimique pour polymériser le PolyRDCZ entre les surfaces plasmoniques et une microélectrode Pt. La réponse couplée électrique et de fluorescence de la jonction a été détectée sous les stimuli d'une excitation plasmonique.

Mots clés: Photophysique, Électrochimie, Microscopie à fluorescence, Microscopie électrochimique à balayage (SECM), Électrofluorochromisme

List of abbreviations

AuNPs	Gold nanoparticles
BFEE	Boron trifluoride-diethyl etherate
BP	Band pass
CA	Chronoamperometry
CCD	Charge couple device
CV	Cyclic voltammetry
DCE	1,2-dichloroethane
DCM	dichloromethane
FITC	Fluorescein isothiocyanate
$\mathbf{I_{EC}}$	Electrochemical current
$\mathbf{I_T}$	Transport current
$\mathbf{I_{tip}}$	Tip Current
IRF	Instrument Response Function
ITO	Indium-doped Tin Oxide
ITO@AuNPs	Plasmonic substrate. ITO with electrodeposited gold nanoparticles
LP	Long pass
LSPR	Localized surface plasmon resonance
NPs	Nanoparticles
OPD	Optical path difference
OVD	Optical volume density
PET	Photoinduced electron transfer
PolyCZ	Polycarbazole
PolyRDCZ	Polymerized (*E*)-4-(2,5-di(thiophen-2-yl)-1*H*-pyrrol-1-yl)-*N*-(pyren-1-ylmethylene)aniline
RDCZ	(*E*)-4-(2,5-di(thiophen-2-yl)-1*H*-pyrrol-1-yl)-*N*-(pyren-1-ylmethylene)aniline dyad molecule
RhB	Rhodamine-B
SECM	Scanning Electrochemical Microscopy
$\mathbf{TBAPF_6}$	Tetrabutylammonium hexafluorophosphate
TCSPC	Time-Correlated Single Photon Counting
TTTR	Time-Tagged Time resolved
UME	Ultramicroelectrode
$\mathbf{V_{sub}}$	Substrate potential
$\mathbf{V_{tip}}$	Tip potential

1. Introduction

Electrofluorochromism (EFC) describes the phenomena of emission modulation with an applied potential and subsequent electrochemical conversion of redox species.[1] Multifunctional materials with reversible switching capacity of both emission and color, have attracted a great deal of interest due to their potential applications as sensors[2, 3], biochemical labels[3], optoelectronic devices[4], and displays[1, 5].

This phenomenon is observed for different classes of materials: switchable molecular dyads, intrinsically electroactive fluorophores, and electroactive (and fluorescent) conjugated polymers.[1, 6] The use of the later ones is particularly attractive due to their conductive properties and because most applications require solid state EFC devices.[6] This property makes these materials interesting for molecular electronics and ideal to build EFC molecular junctions directly between the electrodes by electropolymerization.

Plasmonic substrates are great candidates to add a light-stimulated response to molecular electronic devices. The localized surface plasmon resonance (LSPR) generated by light excitation can allow both tunning of the electromagnetic environment and the charge transport characteristics in the vicinity of the plasmonic substrate.[7] The response of conjugated polymers to this plasmon-induced phenomena is still a topic of study.[4, 8]

The use of EFC conjugated polymers in plasmonic molecular junctions can potentially be used to understand the conductive properties of conjugated polymers in presence of plasmon excitation.[4] This effect can be studied through the coupled electrochemical and fluorescence response collected from the junction. Further leading to future development of molecular electronic devices with a multimodal optical response to electric or light stimuli.

In this study, an EFC conjugated polymer was prepared by electrochemical and photophysical methods and further characterized. Then, a molecular junction was fabricated with this polymer between a Pt ultramicroelectrode and a plasmonic substrate. The aim of the project is to investigate how the conducting properties of a conjugated polymer can be tuned by plasmon excitation, using SECM, fluorescence and optical microscopies as sensitive detection techniques.

In the following introductory sections, a brief scientific context of relevant topics in the current study will be posed to aid the reader have a better comprehension of the report's content.

1.1 Electrofluorochromic system in study: RDCZ dyad

Carbazole (CZ - Figure 1.1a) is a popular precursor for production of conjugated polymers due its chemical stability and functionalization versatility.[9] Typically, CZ can be functionalized easily in the N- position or in the β- carbons while remaining electropolymerizable, to obtain a functionalized conjugated polymer with desired properties (for example: electrofluorochromic behavior).

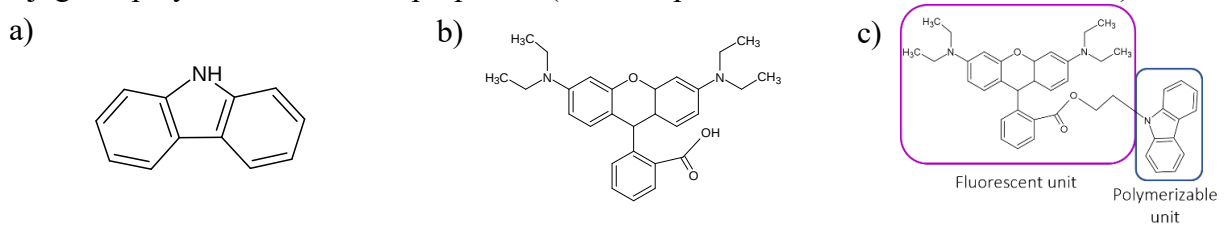

Figure 1.1 (a) Carbazole: CZ (b) Rhodamine-B: RhB (c) RDCZ dyad molecule. IUPAC name: (*E*)-4-(2,5-di(thiophen-2-yl)-1*H*-pyrrol-1-yl)-*N*-(pyren-1-ylmethylene)aniline.

CZ and its derivatives can be polymerized by chemical or electrochemical methods, although the former one tends to be more selective.[10] The polymerization has been found to occur in positions 3, 6 and 9 according to the molecule substitution and external conditions; where position 3 is typically the

most stable.[9, 11] Upon polymerization, they form semiconducting or conducting polymers, which makes them ideal electroactive components for optoelectronic devices.[2, 9, 12]

The electrofluorochromic precursor molecule used in this study is (*E*)-4-(2,5-di(thiophen-2-yl)-1*H*-pyrrol-1-yl)-*N*-(pyren-1-ylmethylene)aniline dyad molecule, refer to as RDCZ in this report. The molecule consists in an electroactive unit (carbazole), a fluorescent unit (Rhodamine-B - Figure 1.1b) and a spacer (C_2H_4 link between the two moieties), as shown in Figure 1.1c.[2]

The polymerization of RDCZ was reported through the oxidation of the carbazole unit by common electrochemical procedures (CV or CA). A PolyRDCZ film was prepared on ITO, which showed electrochromic behavior (switching of color due to applied potential). Nonetheless, no fluorescence studies have been reported for this system.[2]

1.2 Methods for polymerization: Electropolymerization and Photopolymerization

In this study, two polymerization approaches were used to produce PolyRDCZ: electrochemical and photochemical. In this section the principle for each one will be presented shortly.

Electropolymerization

The use of electrochemical methods for the synthesis and characterization of conductive polymers was discovered by Diaz et al in 1979.[13] The polymerization can be achieved by applying a sufficiently positive potential E_{polym} (by chronoamperometry) or by cyclic voltammetry with a sufficiently high anodic limit (usually 0.1-0.2 V above E_{polym}).[14] This polymerization method is typically used for conjugated molecules (for example – carbazole); their oxidation resulting in linear polymer chains.[9]

The polymerization mechanism initiates by the monomer M (HMH – where H in the monomer are explicitly indicated) oxidation on the electrode surface. The subsequential step is the dimerization of the radical species. The further loss of 2 H^+ restores the aromaticity of the dimer. The dimer further oxidizes and reacts with other monomer or dimer molecules forming oligomers (Figure 1.2). The oligomers solubility diminishes rapidly as the chain length increases, resulting in a polymer film on the electrode surface.[9, 13, 14]

$$HMH - e^- \longrightarrow HMH^{\cdot +}$$

$$HMH^{\cdot +} + HMH^{\cdot +} \longrightarrow HMHHMH^{++} \longrightarrow HMMH + 2H^+$$

$$HMMH \longrightarrow\longrightarrow [M]_n$$

Figure 1.2 General scheme for electropolymerization mechanism.[14]

The polymerization rate and film properties depend on experimental conditions such as the monomer concentration, solvent, electrolyte salt, temperature, and pH.[10] Thus, optimization of polymerization conditions is generally required for each system. The electropolymerization approach offers a simple procedure to prepare conductive polymer thin films avoiding the use of extra chemical reactants.

Photopolymerization

Photochemical activation by UV-Vis light irradiation is also a frequently used method to initiate radical mediated polymerization. The process is initiated by generation of reactive species, either free radicals or ions, by excitation of a photosensitive compound. Then, the photogenerated species reacts with the monomer and triggers the polymerization through a radical mechanism; a general scheme of the mechanism is shown in Figure 1.3.[15]

When using dyes (for example – rhodamine) as the photosensitizer compound, the radical generation occurs through photoinduced electron transfer (PET) involving a co-initiator (monomer molecule or another compound). More details regarding this mechanism will be discussed in section 3.2.1.

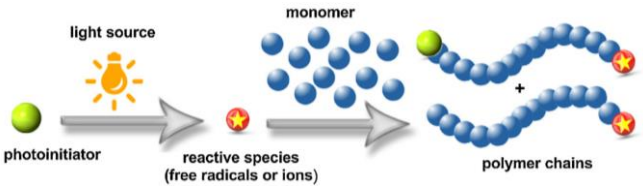

Figure 1.3 General scheme of a photoinitiated polymerization.[16]

This photophysical approach allows polymerization to occur under mild conditions, using less solvent, and with high spatial control. Furthermore, the polymerization rate can be easily controlled [17]by adjusting the photosensitizer concentration and light intensity.

1.3 SECM principle and use for molecular junction fabrication.

Scanning electrochemical microscopy (SECM) is a scanning probe technique used to study electrochemical reactivity of a substrate by using a ultramicroelectrode (UME) tip. A scheme of the SECM set-up is shown in Figure 1.4a.[18] The potential at the tip and substrate is controlled by a bipotentiostat, and the tip position is controlled by a piezo controller. The UME is generally a Pt or C electrode with radii between 1-25 µm sealed in glass.

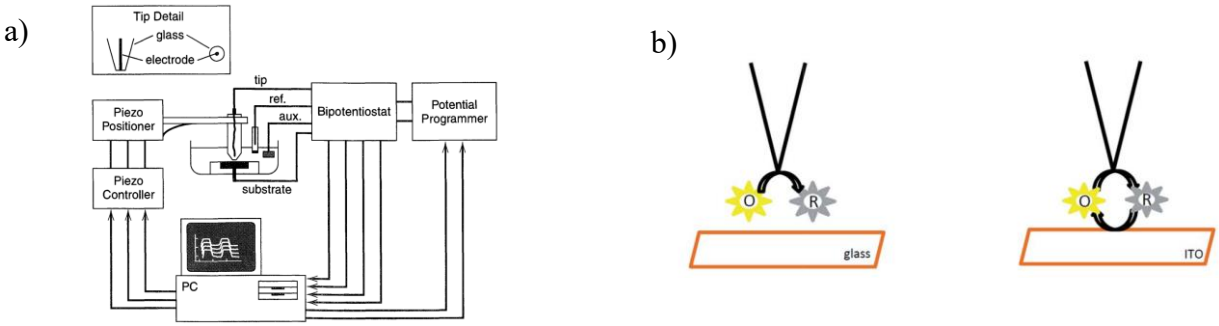

Figure 1.4 (a) Scheme of SECM set-up[18] (b) Principle of SECM in feedback mode. Negative feedback on insulating substrate (left). Positive feedback on conductive substrate (right)[19]

In a SECM experiment, the UME tip and substrate are submerged in a solution containing the electroactive species and a supporting electrolyte. The current at the tip is a function of the reaction rate of species on the electrode surface.[19] When the tip is close to substrate, two scenarios are possible: (1) The substrate is insulating: thus it restricts the diffusion of the oxidated species (O) to the tip (negative feedback) (2) The substrate is conductive: in that case it can regenerate O resulting in a current increase (positive feedback). This operation mode is illustrated in Figure 1.4b.[18]

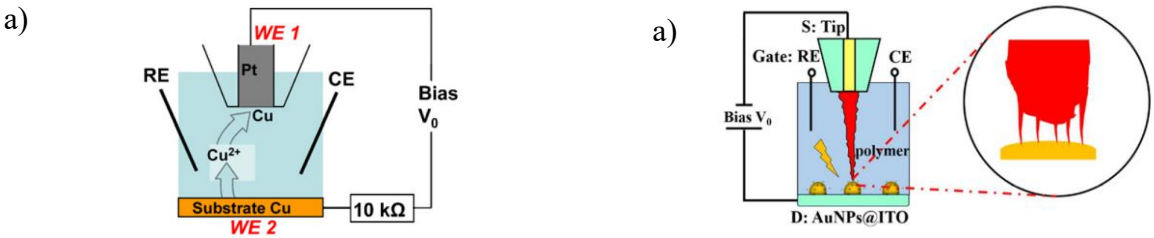

Figure 1.5 Examples of molecular junctions fabricated in a SECM set-up. (a) Scheme of fabrication of copper nanowires.[20] (b) PEDOT junction and close-up of nanowire contact with the AuNPs in the substrate.[4]

Molecular junctions fabricated using SECM set-up have been previously reported[4, 20, 21]. For this procedure a purely electrochemical approach was undertaken. For the fabrication of Cu nanowires (Figure 1.5a), a potential bias is applied between the two electrodes leading to Cu^{2+} dissolving from the anode (substrate) and depositing on the cathode (tip) until a connection is established.[20] For the polymer junction (Figure 1.5b), a sufficiently positive potential is applied on the tip to generate

electropolymerization until the growing polymer contacts the substrate. This geometry then allows to switch the polymer between neutral and oxidized state by applying a voltage bias.[4]

1.4 Introduction to plasmonics and its interactions with fluorescent systems

The interaction of the electromagnetic field of light with the surface electrons in metallic nanoparticles produces a collective oscillation of the conduction electrons. (Figure 1.6a) This phenomenon is known as localized surface plasmon resonance (LSPR) and occurs when the metallic nanoparticles dimensions are smaller than the wavelength of the incident light.[17, 22] LSPR is strongly related to nanoparticle size. For larger nanoparticles, the LSPR peak broadens and shifts to higher wavelengths (red shift) due to higher order oscillations and less repulsions of the electrons. (Figure 1.6b)[23]

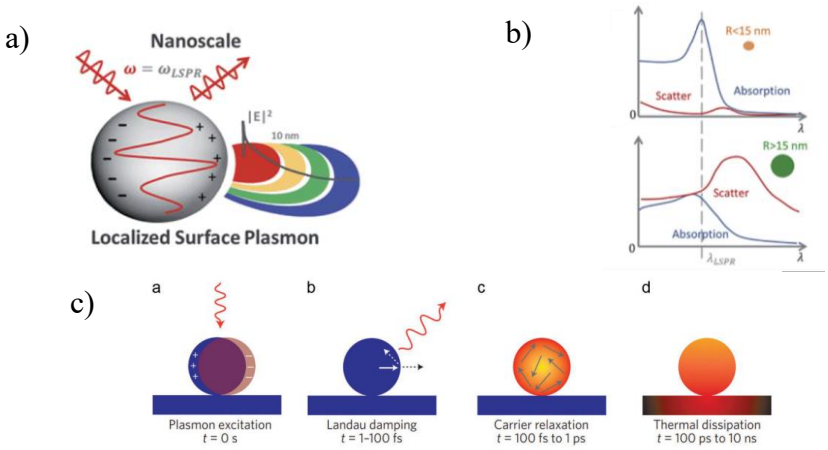

Figure 1.6 (a) Localized surface plasmon resonance - LSPR[17] (b) Absorption and scattering dependence on nanoparticle size.[17] (c) Photoexcitation and relaxation process of LSPR in metallic nanoparticles.[22]

Several phenomena can be induced during the photoexcitation of LSPR in metallic nanoparticles (Figure 1.6c). a- Upon irradiation the collective oscillation of electrons generates LSPR, these confined electrons generate an enhancement of the electromagnetic field (several orders of magnitude higher than the incident light). b- The highly energetic LSPR decays through light remission; c- or through hot charge carrier (holes and electrons) generation and relaxation. d- Thermal dissipation generating local heating in the vicinity of the nanoparticle.[22]

Fluorescence is known to be sensitive to plasmon-induced phenomena. Near the metallic surface (≤ 10 nm), a fluorophore interacts directly with electrons on the metallic surface. When there is an overlap between the NPs absorption and the fluorophores emission, an energy transfer process occurs resulting in fluorescence quenching.[24] Outside the quenching zone, the coupling of the enhanced electromagnetic field with the fluorophore excitation can generate fluorescence enhancement. Nonetheless, this effect decays rapidly with increasing distance to the metallic surface.[23] Therefore, the quenching or enhancement nature of plasmon is dependent on the fluorophore distance to the metallic surface, as shown in Figure 1.7. Other factors such as NP size, shape, and material, as well as the nature of the fluorophore will have a strong effect on this fluorophore-plasmon interaction.[17]

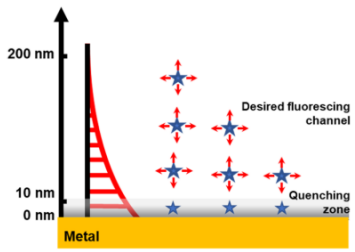

Figure 1.7 Distance dependency of the interaction of fluorophores with metallic nanoparticles.[23]

2. Materials and Methods

2.1 Chemicals and Materials

All chemicals used in this research were of analytical grade without further purification. Rhodamine B 95%, Carbazole >95%, Boron trifluoride-diethyl etherate (BFEE), and Gold(III) chloride trihydrate >99.9% from Sigma-Aldrich, dichloromethane (DCM) and 1,2-dichloroethane (DCE) from Carlo Erba Reagents, tetrabutylammonium hexafluorophosphate 98% ($TBAPF_6$) from TCI Chemicals, sodium carbonate (Na_2CO_3) from Prolab, ultrapure milli-Q water. For electrodeposition, the substrates used were 10x30mm or 25x25mm ITO-coated glass plates from Solems previously rinsed with ethanol.

The (*E*)-4-(2,5-di(thiophen-2-yl)-1*H*-pyrrol-1-yl)-*N*-(pyren-1-ylmethylene)aniline dyad molecule, referred to as RDCZ during this study, was synthetized by Dr. U. Darbost (IUT de Lyon).

2.2 Electropolymerization of RD-CZ system

The PolyRDCZ film on ITO was synthesized via the cyclic voltammetry (CV) or via chronoamperometry (CA) techniques. A three-electrode cell assembly was utilized with a reference electrode (Ag wire), counter electrode (Pt wire), and working electrode (ITO). The electrochemical cell was filled with a solution containing 0.1M RDCZ dyad + 3% of pure carbazole (CZ), dissolved in DCM+BFEE as solvent (1 drop of BFEE per ~2mL of solution), and 0.1 M $TBAPF_6$ as a supporting electrolyte. The RDCZ solution exhibited a bright pink color. Electropolymerization was achieved via CV by cycling the potential between 0.3 V and 1.5 V for five cycles at a scan rate of 0.1 V s^{-1}. It was also achieved via chronoamperometry by applying 1.5V for 60s.

After polymerization, the polymer film on ITO was rinsed with DCM and ethanol. The electrochemical characterization of PolyRDCZ was performed by CV in DCM+0.1M $TBAPF_6$ solution (dyad free). The measurements were performed with a CH Instruments potentiostat.

2.3 Coupled electrochemical and optical microscopy set-up

All spectroelectrochemical and Scanning Electrochemical Microscopy (SECM) experiments were conducted in a set-up coupling and electrochemical cell with an inverted microscope as shown in Figure 2.1.

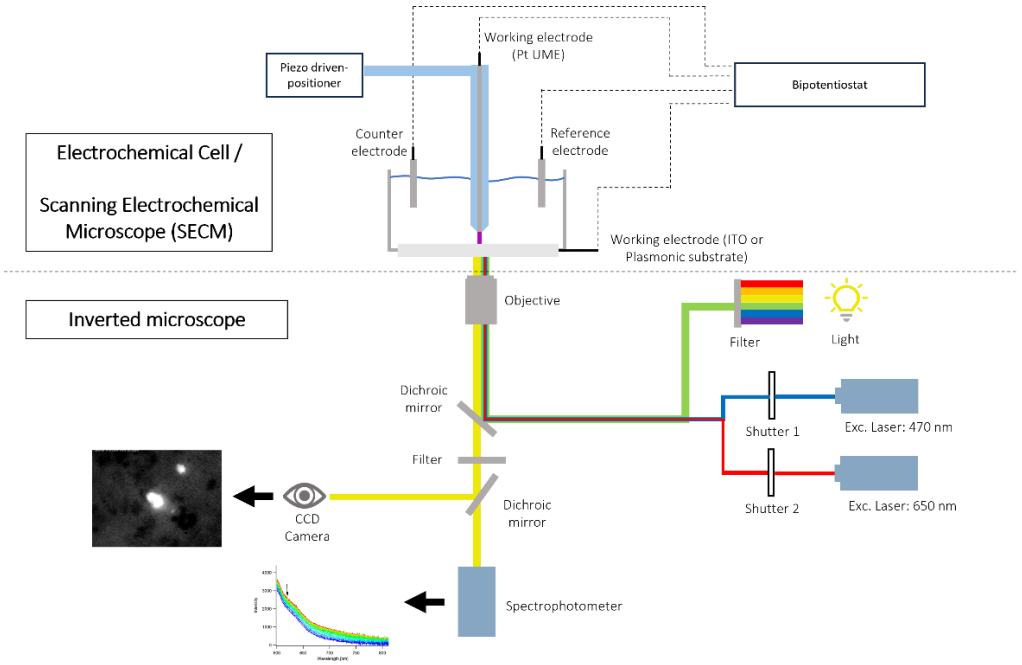

Figure 2.1 Experimental set-up for coupled electrochemical and optical experiments.

Electrochemistry - Electrochemical measurements were performed using a homemade spectroelectrochemical cell on top of an inverted optical microscope. A platinum wire and an Ag wire were used as the counter and reference electrodes, respectively. The set-up was used in the standard three-electrodes configuration or in four-electrodes bipotentiostat configuration (SECM) according to the experiment. In the three-electrode configuration a transparent conductive substrate (ITO) was employed as the working electrode. In the four-electrode configuration a Pt ultramicroelectrode (UME) was added as second working electrode in bipotentiostat mode. Measurements were carried out with a VersaSTAT 4 and VersSTAT 3 (Ametek) potentiostats driven by VersaStudio software (Ametek)

Optical measurements - Measurements were performed on an inverted microscope (Ti Eclipse Nikon) with a 40× NA 0.60 objective in a wide-field epi-illumination configuration. Excitation source is a Hg lamp (Intensilight Nikon) with a band pass excitation filter (BP 561-14 nm) and m-Cherry dichroic mirror. Two other lasers can be used as excitation sources: a pulsed laser diode at 470 nm (LDH-P-C-470B, 40MHz, 150 ps-fwhm, Picoquant), and a supercontinuum laser filtered at 650 nm ±7 nm (SMHP-40.2A-PP-RC, 50 ps-fwhm,10 MHz, Leukos) with a respective FITC dichroic mirror or a multiband dichroic mirror (492-30,564-15,640-15). The excitation sources used for each experiment were selected by opening and closing the respective shutters controlled manually or through MATLAB. Emitted light is collected through a long pass emission filter LP593 nm or LP520 nm, or BP575-25, according to the experiment. Acquisition time-lapses are carried out using a CCD Pixel Fly camera from PCO under the μManager open source software. Emission spectra are recorded with an Ocean Optics spectrometer coupled to the microscope with an UV-Vis (400 μm diameter) optical fiber plus collimator placed in an intermediate image plane, with a 60 μm mode field diameter in the sample plane centered around the tip.

2.4 Photophysical studies in solution

Absorption and Emission spectra - Absorption spectra were recorded using a Cary Series UV−visible spectrophometer Cary-5000 in 10 mm quartz cuvettes from M&B Thuet France. The concentrations of the solutions were ~1 μM in dichloromethane for rhodamine-B and RDCZ. The emission spectra were recorded with a Fluorolog from Jobin Yvon HORIBA; 560 nm was used as excitation wavelength with a slit of 1.5 nm for both excitation and emission.

Lifetime measurements - Fluorescence decay curves are obtained by the time-correlated single-photon counting (TCSPC) method. The setup is made of a titanium sapphire Ti:Sa oscillator (Spectra Physics, Maï Taï) emitting pulses of 100 fs duration at 940 nm (80 MHz frequency). The repetition rate is reduced to 4 MHz by a pulse picker, and non-linear SHG crystal generates the desired wavelength at 470 nm (GWU Lasertechnik, UHG-23-PSK). Emitted photons are collected at 90° through a polarizer at the magic angle and a monochromator at 580 nm ± 10nm. Incoming photons are collected with a micro-channels plate photomultiplier (MCP-PMT R3809U-50, Hamamatsu) and processed with a TCSPC module (SPC-630, Becker & Hickl) where global IRF resolution is 40 ps. Decays are adjusted by a one or a bi-exponential function with minimization of $\chi 2$ using nonlinear least-squares Lenvenberg−Marquardt method [25] under Igor Pro Wavemetrics Inc. software.

2.5 Photopolymerization of RDCZ

All photopolymerization experiments were conducted on a modified version of the set-up described in section 2.3, shown in Figure 2.2.

The grafting solution (0.01 M of RDCZ in DCM) is kept in a 10 μm thin cell (Hellma) or in a homemade cuvette. An excitation laser (470 nm pulsed laser) is introduced through the backport of the microscope and focused at the substrate-liquid interface using an objective lens (100× oil immersion

NA = 1.49 when using the microcuvette, or 40× NA=0.60 when using the homemade cuvette), then the image is built with a 1.5× tube lens and a 2.5× relay lens system (C-Mount TV Relay Lens VM 2.5×). The sample is illuminated in transmission using red light through a band pass 633nm±10.

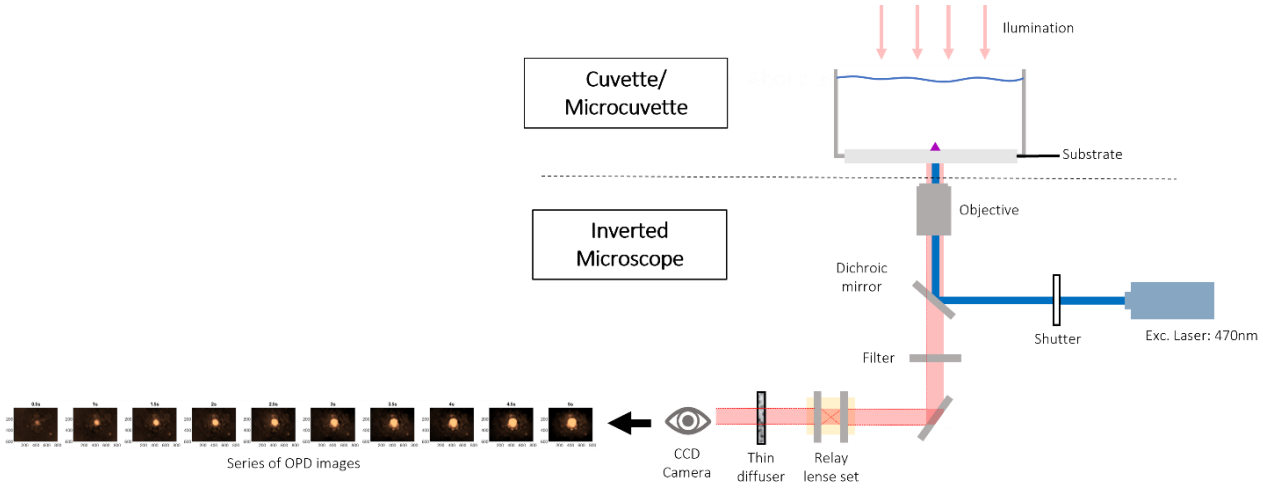

Figure 2.2 Experimental set-up used for photopolymerization.

The quantification of the thin polymer layer is achieved through quantitative phase imaging, using a Diffuser-based Phase Sensing and Imaging (DIPSI) imaging system previously reported by the group.[26] In this implementation, a thin diffuser is located between the microscope exit and the CCD camera at a d=3 mm, generating a random interference pattern(a speckle pattern). The polymer is grafted by excitation with the laser with cycles of interruptions for phase image acquisition (typically 1000 ms). As the incident light leads to polymerization, a layer of high refractive index is formed, which generates an optical path difference (OPD) between a reference image (an image taken before the polymerization) and the phase image.[26, 27] The relation between the OPD and the actual object thickness (L)is given by OPD = Δn × L, where Δn is the refractive index difference between the growing layer and the medium.[28] The formation of the polymer can then be observed as a series of OPD images.

The OPD images are integrated over the region of interest (ROI) in each phase image, leading to the total optical volume (OVD).[28] An Arduino board is used to manage the acquisition of phase images and control the laser exposition. The data analysis was performed with MATLAB.

To build micro/nano structures by photopolymerization, the microscope stage is moved by a E-727 Digital Piezo Controller which is controlled by MATLAB. This method allows to produce complex structures with PolyRDCZ. The polymerization was performed on glass and ITO.

2.6 Atomic Force Microscopy (AFM)

The photopolymerized microstructures were characterized by AFM using a Icon Dimension Atomic Force Microscope (Bruker) equipped with Si PointProbePlus tips (PPP-NCHR, NanoSensors) operated on tapping mode.

2.7 Fourier-transform infrared spectroscopy (FTIR)

ATR-FTIR analysis was carried out on a Nicolet iS50 FT-IR (Thermo Scientific) spectrometer. Air was used as a background spectrum. The photopolymerized PolyRDCZ sample consisted of a square grid of dots (200x200 µm and 50 nm thickness) on a thin glass slide. The electropolymerized PolyRDCZ sample was a thin film (~150 nm thickness) on a thin ITO slide. Spectra were recorded with a total of 32 scans.

2.8 Molecular junction between two gold electrodes and determination of conductivity

A molecular junction of PolyRDCZ was prepared via photopolymerization by direct writing with a 470 nm laser on glass substrate between two gold electrodes (Prepared by lithography by Dr. Rasta Ghasemi), using the experimental set-up described in section 2.5 (Figure 2.2). The grafting solution was 0.01 M RDCZ+10% CZ in DCM.

The resistance of the junction was determined by applying a potential bias between the two gold electrodes in a cyclic voltammetry experiment (0 V to 0.5 V, 7 cycles, increasing scan rate from 0.01 V/s to 0.5 V/s) using a two-electrode configuration. The dimensions of the junction were measured by AFM. The conductivity was then calculated as shown in equation 1; where c is conductivity (S cm^{-1}), ρ is resistivity (Ω cm), L is length (cm), A is transversal area (cm^2), and R is resistance (Ω).

$$c = \frac{1}{\rho} = \frac{L}{R \cdot A} \qquad [1]$$

2.9 Building molecular junction between a Pt ultramicroelectrode and a plasmonic substrate

A molecular junction in a vertical configuration was fabricated using the experimental set-up described in section 2.3. The SECM was used in a four-electrode configuration, a Pt UME as the first working electrode, and a plasmonic substrate as the second working electrode.

The plasmonic substrate consisted in an ITO coated with gold nanoparticles (ITO@AuNPs). It was fabricated by electrodeposition of a gold source solution (2 mM Gold(III) chloride trihydrate in ultrapure Mili-Q water + 0.1 M Na_2CO_3 as supporting electrolyte) on ITO through chronoamperometry, using conditions previously optimized by the group (-0.9 V for 300 s). The chronoamperometry and absorbance spectrum for the ITO@AuNPs substrate are shown in Figure 2.3.

The junction was achieved using a photo/electrochemical approach. First, a PolyRDCZ column (~20 µm) was prepared on the plasmonic substrate by photopolymerization by moving the piezo stage down in Z-axis using a 470 nm laser for excitation (section 2.5). Then, the Pt UME was approach and pressed to the PolyRDCZ column until 10 µm from the substrate. To complete the connection, electropolymerization was performed by applying a CV on the tip (0.3 V to 1.5 V, for ~40 cycles). The effect of plasmonic excitation was tested by applying different V_{tip} and V_{sub} while applying ON/OFF cycles of plasmonic excitation using a 650 nm laser focused (Average power density: 1 kW/cm^2) on the AuNPs. The junction response was measured as changes in I_{tip} and fluorescence. A 0.01 M RDCZ+10 % CZ solution in DCM+0.1M $TBAPF_6$ was used for the fabrication procedure; all further testing was also performed in presence of this solution. The fluorescence was recorded with a CCD camera adjusting the ROI to the area covered by the junction.

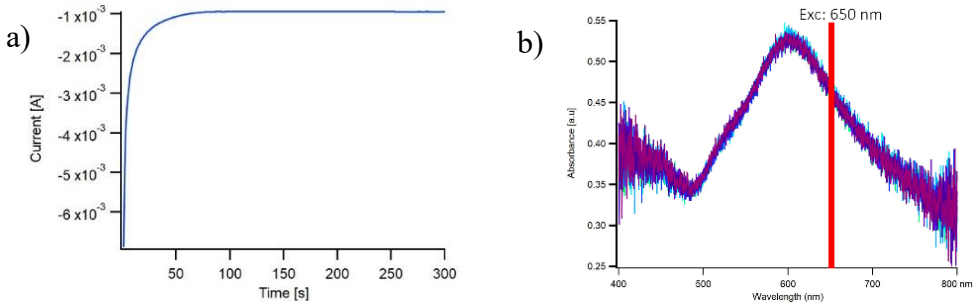

Figure 2.3 (a) Chronoamperometry of electrodeposition of Au nanoparticles on ITO. Potential: -0.9 V (b) Absorbance of the ITO@AuNPs substrate. Supercontinuum laser used for plasmonic excitation: 650 nm.

3. Results

The study is divided into three parts; first the electrofluorochromic properties of PolyRDCZ will be explored by preparing the polymer by electrochemical methods. Then, the polymerization of the RDCZ dyad is also explored by a photophysical approach which allows micro/nanofabrication of complex structures with high spatial resolution. Finally, a photo/electrochemical approach is used to fabricate a molecular junction between a Pt ultramicroelectrode (Pt UME) and a plasmonic substrate (ITO@AuNPs). This geometry is used to study the effect of plasmonic excitation on the conductive properties of the polymer.

3.1 Electropolymerization and electrofluorochromic characterization of PolyRDCZ system

3.1.1 Electropolymerization of RDCZ

The electropolymerization of carbazole and its derivatives is a widely used method to fabricate conductive polymer thin films.[9, 10, 12, 29] A general scheme of the electropolymerization process and the reported mechanism[10] for carbazole polymerization is shown in Figure 3.1. The oxidation of carbazole consists in a one electron transfer to form a cationic radical. This radical is rather unstable and therefore it rapidly couples with another cation or radical to form the more stable dicarbazyl molecule; the formation of this molecule is accompanied by the loss of two protons. The coupling can lead to 3,3′-bicarbazyl (D) as main product and several minor products (2,2'-, 4,4'-, 5-5'-, and 9,9′-bicarbazyl). After, the oxidation of the oligomers leads progressively to the formation of a polycarbazole (PolyCZ) film on the electrode surface. The RDCZ dyad used in this study is an N-substituted carbazole derivative, therefore the polymer is expected to form only through the 3,3′bicarbazyl intermediate.

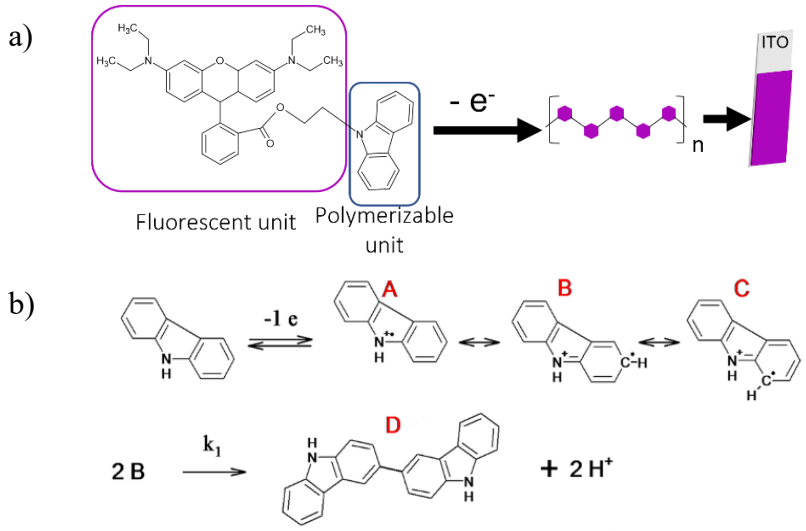

Figure 3.1 (a) Scheme of electropolymerization on ITO coated glass (b) Reported mechanism for carbazole electropolymerization.[10]

Typical CV curves showing the electro-oxidation of RDCZ into a PolyRDCZ thin film on ITO are shown in Figure 3.2. Surprisingly, early attempts to electropolymerize RDCZ were unsuccessful, prompting a revision of the electropolymerization protocol. Suspecting that the RhB group could exert steric hindrance on the system, higher concentrations of RDCZ were used (0.01-0.1 M). Furthermore, increasing amounts of pure CZ were added to trigger the polymerization, until a uniform film with the desired electrochromic properties was obtained. For the electrochemical characterization a 0.1 M RDCZ + 3 % CZ solution was used since it allowed easier detection of the redox peaks. Further

spectroelectrochemical studies were performed with a 0.01 M RDCZ+10 % CZ solution; the polymer properties were similar using either one of these conditions.

The onset potential for the polymerization was observed at ~ 0.9-1 V vs Ag; which coincides with the reported values for other similar carbazole derivatives.[2, 12, 30] Post-polymerization, the PolyRDCZ film was characterized by CV in a pure electrolyte solution (no dyad present). The current showed a decrease after the first cycle but then stabilized after further cycling (Figure 3.2). This could be explained by a release of RDCZ dyad adsorbed on the polymer film; which agrees with a light pink color observed in the electrolyte solution after the first few cycles of the CV.

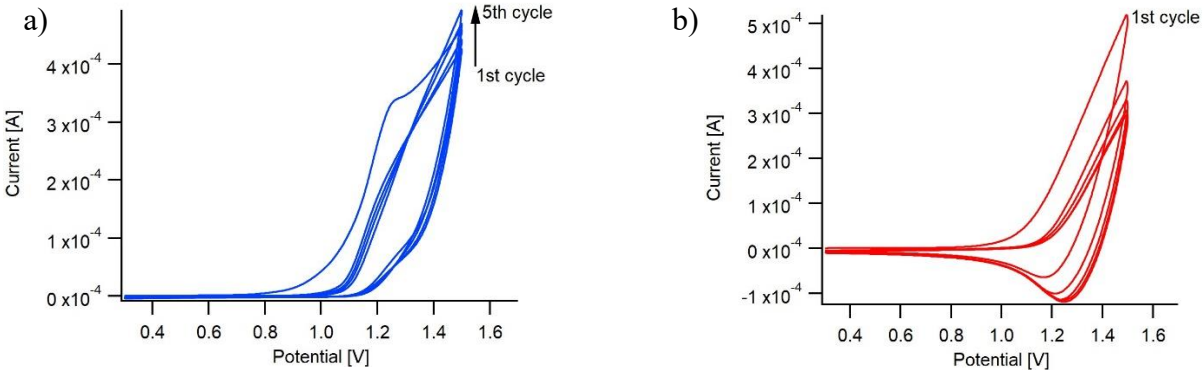

Figure 3.2 (a) Electropolymerization of RDCZ via cyclic voltammetry. CV: 0.3 V to 1.5 V, 5 cycles, 0.1 V/s. Solution: 0.1 M RDCZ + 3% CZ in DCM+0.1M $TBAPF_6$. (b) Cyclic voltammetry post-polymerization of PolyRDCZ on ITO on a DCM+0.1M $TBAPF_6$ solution (dyad free). CV: 0.3 V to 1.5 V, 5 cycles, 0.1 V/s. Working electrode: ITO. Reference electrode: Ag wire. Counter electrode: Pt wire.

3.1.2 Characterization of PolyRDCZ prepared by electropolymerization

The chemical characterization of the PolyRDCZ thin film on ITO was performed through IR spectroscopy, as shown in Figure 3.3. The presence of the RDCZ moiety was confirmed by the peaks at 1715 cm^{-1} associated to the carbonyl group of RhB, and at 1587 cm^{-1} and 1418 cm^{-1} associated to the aromatic rings. The broad peak at 1125 cm^{-1} is attributed to doping due to the incorporation of the electrolyte $TBAPF_6$ in the film.[2]

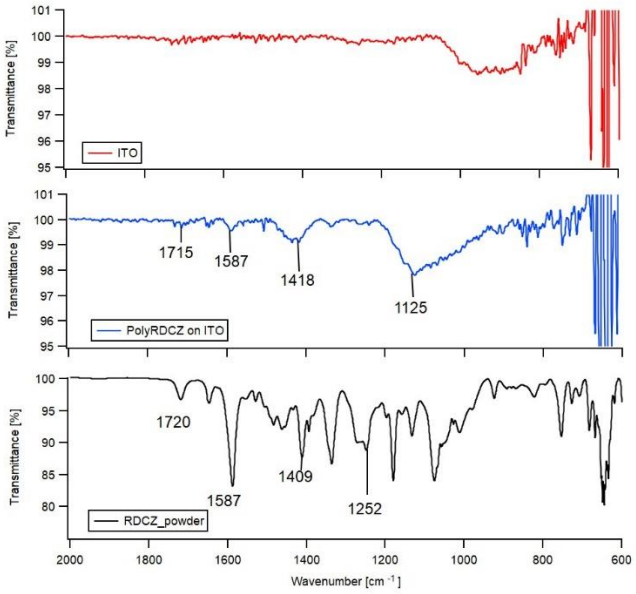

Figure 3.3 FTIR spectra of ITO (top), PolyRDCZ on ITO (middle), and RDCZ dyad (bottom). Sample for PolyRDCZ: Thin film (~150 nm) on a thin ITO-coated glass, prepared by CA at 1.5 V for 60 s.

The PolyRDCZ film was further characterized by CV at increasing scan rates in a dyad free solution, as shown in Figure 3.4. The peak current was then plotted as a function of the scan rate, showing a linear behavior.

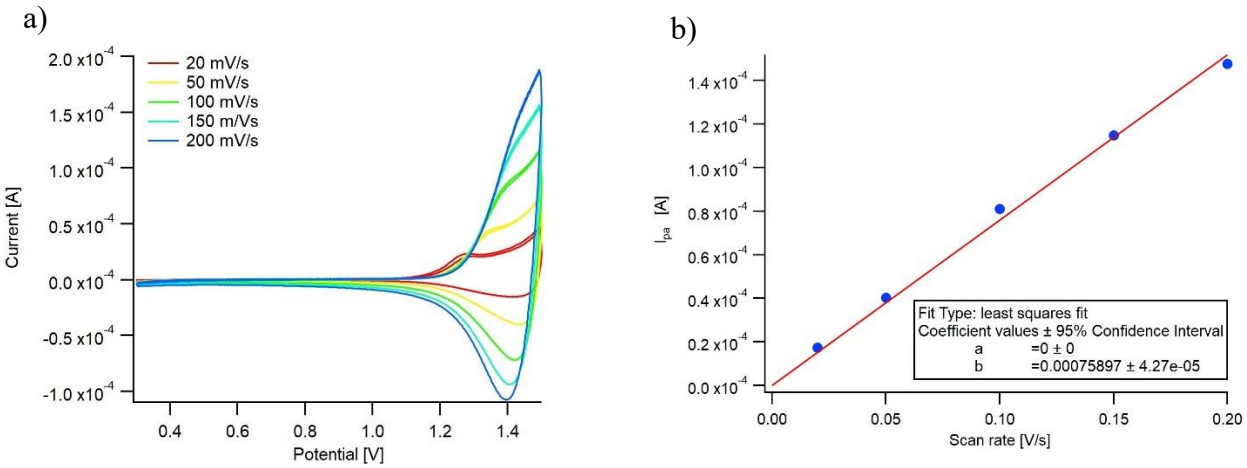

Figure 3.4 (a) Cyclic voltammetry of PolyRDCZ on ITO at increasing scan rates. Solution: DCM+0.1 M $TBAPF_6$ (dyad free). (b) Linear fit of i_{pa} vs scan rate. The intercept was fixed to 0.

For a thin film adsorbed on the electrode surface, the peak current shows a proportionality to the scan rate as shown in equation 2,[14, 18, 31] where i_p is the peak current, n is the number of electron transferred in the redox event, υ (V/s) is the scan rate, A (0.72 cm^2) is the electrode surface area, and Γ_o^* (mol cm^{-2}) is the surface coverage of the adsorbed species.

$$\boldsymbol{i_p = \frac{n^2F^2}{4RT}\upsilon A\Gamma_o^*} \qquad \textbf{[2]}$$

The linear fit (Figure 3.4b) indicates a redox process limited by the number of electroactive sites with a surface coverage of $\Gamma_o^*=1.1\times10^{-9}$ mol cm^{-2} which corresponds to a thin film.[31] However, such analysis assumes fast kinetics, adsorption equilibrium in the film, homogenous distribution of oxidized and reduced species, and non-dependency of Γ with potential which are not entirely met by this system.[18] Furthermore, the oxidation peak is ill-defined making the analysis more challenging. An ideal film absorbed on an electrode should show a symmetrical CV and $E_{pa}=E_{pc}$, not observed in this system. This indicates a deviation from ideality which may be originated by complex factors in the film such as inhomogeneity, finite mass and charge transport through the film, and structural and resistive changes during oxidation.[14, 18]

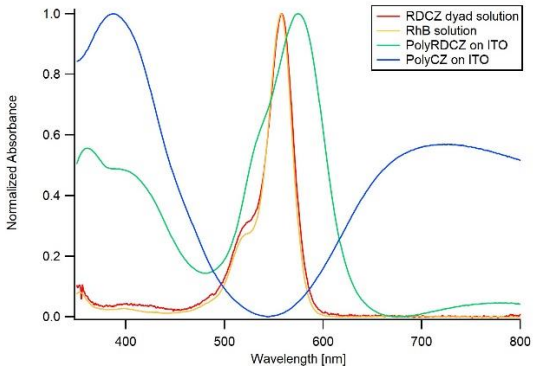

Figure 3.5 Absorption spectra for a RDCZ solution in DCM (1 μM), PolyRDCZ on ITO, and PolyCZ on ITO.

The absorption spectrum of PolyRDCZ on ITO was recorded ex-situ and compared to its RDCZ dyad precursor and to pure PolyCZ on ITO (Figure 3.5). The polymer film shows a λ_{max} = 575 nm, showing a modest red shift with respect to the RDCZ dyad (λ_{max} = 558 nm); the main peak corresponds to the

rhodamine-B moiety. Polymerization also leads to the emergence of a new peak, located around 450 nm which is assigned to the PolyCZ chain in the polymer, based on the absorption spectrum of pure PolyCZ. It is also noteworthy that PolyCZ shows a large bipolaronic band in NIR (650-800 nm), which is evidence of doping in the film. In the case of PolyRDCZ, this band is smaller signifying the film is less doped.

3.1.3 Spectroelectrochemical studies

The conjugated polymer film in this study incorporates an electroactive (carbazole) and a fluorescent (rhodamine-B); thus making possible the electrochemical modulation of both the color and fluorescence by changing the redox state of the polymer.[3]

The electrochromic and electrofluorochromic behavior of the PolyRDCZ film on ITO is verified by conducting spectroelectrochemical experiments in the set-up described in section 2.3. The PolyRDCZ-coated ITO was installed in a homemade electrochemical cell on top of an inverted microscope. Then, using a three-electrode configuration, a CV was performed in pure electrolyte solution. Simultaneously, the absorbance or fluorescence spectra were recorded using a coupled spectrophotometer. This configuration allows to follow the color and emission switching of PolyRDCZ in real-time during the electrochemical experiment.

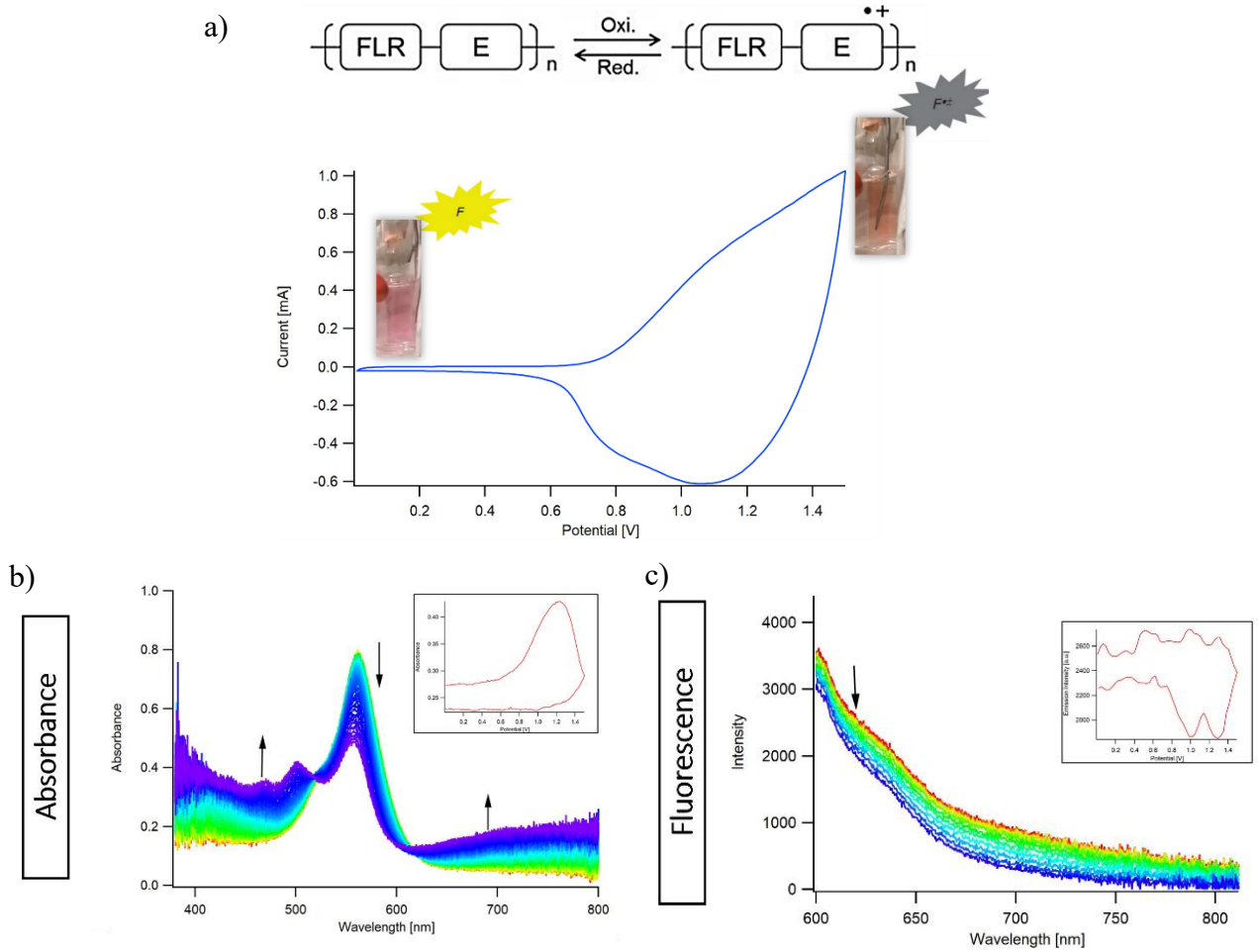

Figure 3.6 Electrofluorochromic and electrochromic modulation of the PolyRDCZ film on ITO. (a) Scheme of electrochromic and electrofluorochromic behavior of PolyRDCZ. Neutral state: Pink, fluorescent. Oxidated state: Orange, quenched fluorescence. (b) Absorbance modulation in oxidation from 0.3 V to 1.5 V. Inset: Absorbance at 500 nm during full CV experiment. (c) Fluorescence modulation in oxidation from 0.3 V to 1.5 V. Inset: Emission intensity at 615 nm during full CV experiment.

The electrofluorochromic modulation, during the oxidation of the PolyRDCZ film (cycling from 0.3 V to 1.5 V) is shown in Figure 3.6. On its neutral state the film shows a pink color, which switches to orange when oxidized at 1.5 V. During the oxidation process, the fluorescence intensity of the film is also observed to decrease. The absorbance spectra showed a change in three distinct peaks: 400-500 nm (increase), 560 nm (decrease), and 700-800 nm (increase). Two isosbestic points were also observed at 520 nm and 610 nm. The change in the absorption bands is generated due to the separation of the HOMO and LUMO bands caused by the electrochemical injection of charges, which leads to the formation of new energy levels know as polarons.[2, 3]

The fluorescence quenching is due to the formation of these polarons or charged species in the electroactive moiety of the polymer (carbazole). These species act as quenching centers by introducing non-radiative pathways for de-excitation through intramolecular charge transfer processes.[3]

3.2 Photopolymerization of RDCZ

The previous electrochemical approach is very useful to produce uniform thin films of PolyRDCZ. In comparison, photopolymerization offers local spatial control allowing micro/nanofabrication of complex structures as well as a fine control of the layer thickness. The oxidation potential of RDCZ suggests that the polymerization of the RDCZ dyad can also be photochemically triggered using the photoactive RhB unit as a sensitizer.

3.2.1 Mechanism

To understand the mechanism behind the RDCZ photopolymerization, the system was studied as separated RhB and CZ (not covalently bonded). Indeed, the excited state redox potential of a Rhodamine-B sensitizer is expected to lead to a photo induced electron transfer (PET); as shown in Figure 3.7.

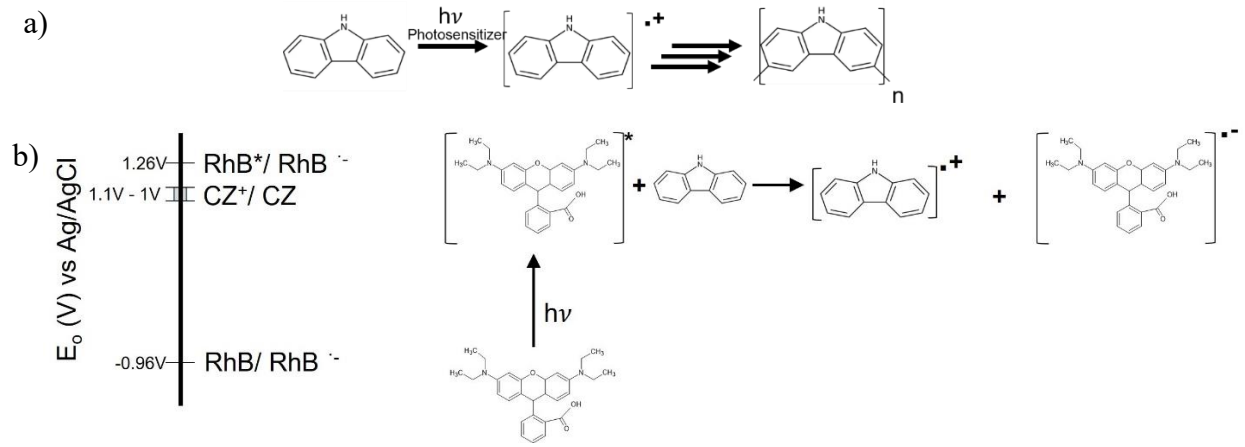

Figure 3.7. (a) Polymerization mechanism of carbazole triggered by a photosensitizer. (b) Photoinduced electron transfer (PET) between rhodamine-B and carbazole

Polymerization of carbazole and its derivatives through an anodic mechanism has been extensively reported in literature.[9-11] Through cyclic voltammetry experiments the apparent oxidation potential for carbazole (E_0^{CZ}) was determined as 0.98 V vs Ag/AgCl. Therefore, RhB fulfills the photoelectrochemical criteria to be a suitable sensitizer for carbazole photopolymerization: (1) $E_0^{GS}(RhB/RhB^-) < E_0(CZ^+/CZ)$ to avoid the ground state reaction, and (2) $E_0^{ES}(RhB^*/RhB^-) > E_0(CZ^+/CZ)$, to enable the RhB excited state to photooxidize the carbazole moiety.[32, 33] Therefore, an electron transfer occurs between the excited sensitizer molecule (RhB*) and a ground state molecule (CZ), generating a carbazole radical ($CZ^{\cdot+}$) which triggers the photopolymerization.

To confirm the photoinduced electron transfer mechanism, the emission of RhB was recorded in presence and in absence of CZ, as shown in Figure 3.8; where I_o is the emission intensity in absence of CZ and I is the emission intensity of the mix solution.

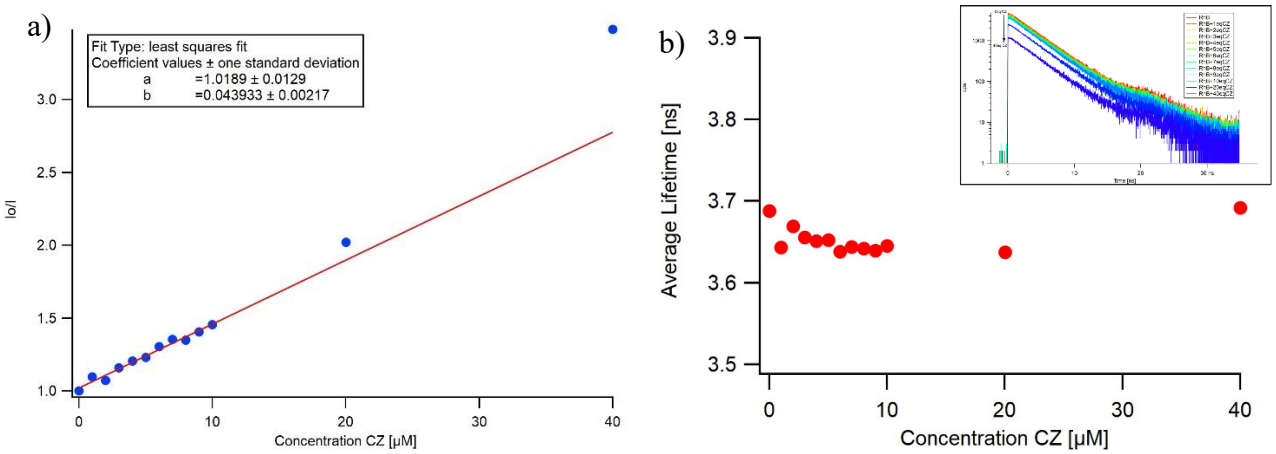

Figure 3.8 (a) Stern-Volmer plot and (b) Average emission lifetime for a 1 µM Rh-B solution in DCM with increasing CZ concentration. Inset: Lifetime measurements by TCSPC.

The Io/I ratio is shown to follow a linear behavior at low concentrations (<10 µM CZ), in accordance with the Stern-Volmer model shown in equation 3; were I_o is the emission intensity of RhB in absence of a quencher, I is the emission intensity in presence of a quencher (CZ), and [CZ] is the carbazole concentration.[33]

$$\frac{I_o}{I} = 1 + K_S[CZ] \qquad [3]$$

In such case, the Stern Volmer proportionality constant is equal to the association constant of the ground state molecules (K_S=[RhB-CZ]/[RhB][CZ]= 4.4×10^4 M^{-1}). These results confirm CZ can act as fluorescence quencher. Furthermore, the average emission lifetime seems to be independent of the CZ concentration, suggesting an static quenching mechanism.[33]

At higher concentrations, the behavior of the Stern-Volmer plot deviates from linearity, suggesting more complex interactions take place. Furthermore, the solution with separated RhB+CZ was observed to evolve over time. The absorbance of the RhB+CZ solution decreased 10 % after 13h from preparation, while the RDCZ dyad solution is stable with less than 1% decrease (Figure 3.9). This confirms the use of the RDCZ offers better stability and decreases the complexity of the photopolymerization process.

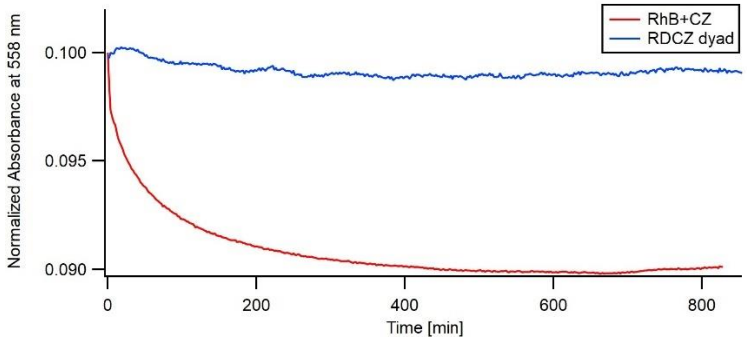

Figure 3.9 Stability studies. Evolution of absorbance peak at 558 nm during 800 min (~13 h) for a 1 µM RDCZ dyad (blue) and separated RhB + CZ (red). Solvent: DCM.

The photopolymerization of the system was tested using a 0.01 M solution in DCE in a microcuvette mounted on an inverted microscope. The solution was illuminated with a focused laser at 470 nm to

achieve polymerization. The growth of the polymer was observed by phase imaging both for a mixture of RhB + CZ (no covalent bond) and for the RDCZ dyad (Figure 3.10), confirming the role of RhB as sensitizer. Nonetheless, the photopolymerization process is clearly more efficient by using the RDCZ dyad, as the emergence of the polymer requires less exposure time to the excitation laser. Carbazole alone did not polymerize by sole light excitation even using a higher power and longer exposure time.

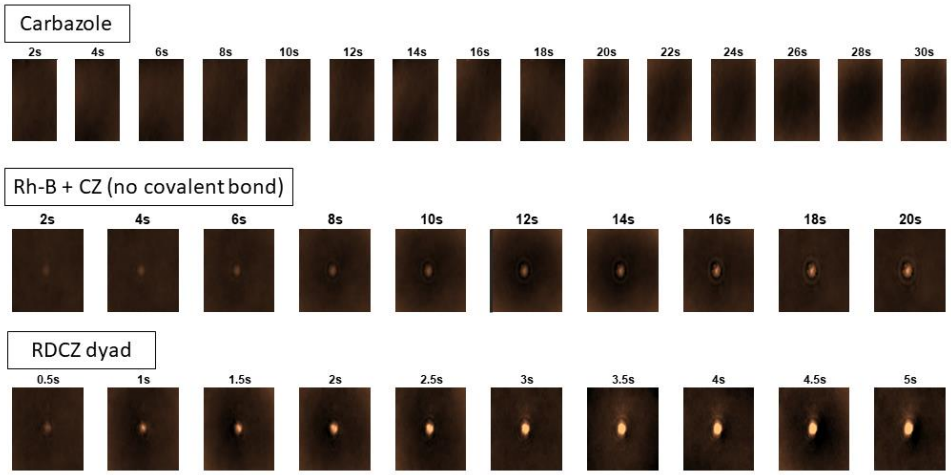

Figure 3.10 Phase images of photopolymerization sequence. The appearance of a growing polymer is observed only in the presence of rhodamine-B as sensitizer. Samples: 0.01 M solution in DCE in a microcuvette (Height=10 µm) mounted on top of an inverted microscope. Magnification:100×1.5×2.5×. Substrate: Glass. Carbazole (Power: 500 µW, Exposure time: 30 s). RhB+CZ (Power: 150 µW, Exposure time: 20 s). RDCZ (Power: 150 µW, Exposure time: 5 s)

3.2.2 Characterization of PolyRDCZ prepared by photopolymerization

The chemical characterization of the PolyRDCZ grafted on glass was performed through IR spectroscopy (Figure 3.11). The sample prepared for this experiment was a grid of dots of 200x200 µm and 50 nm thickness, with the purpose of covering the maximum area possible.

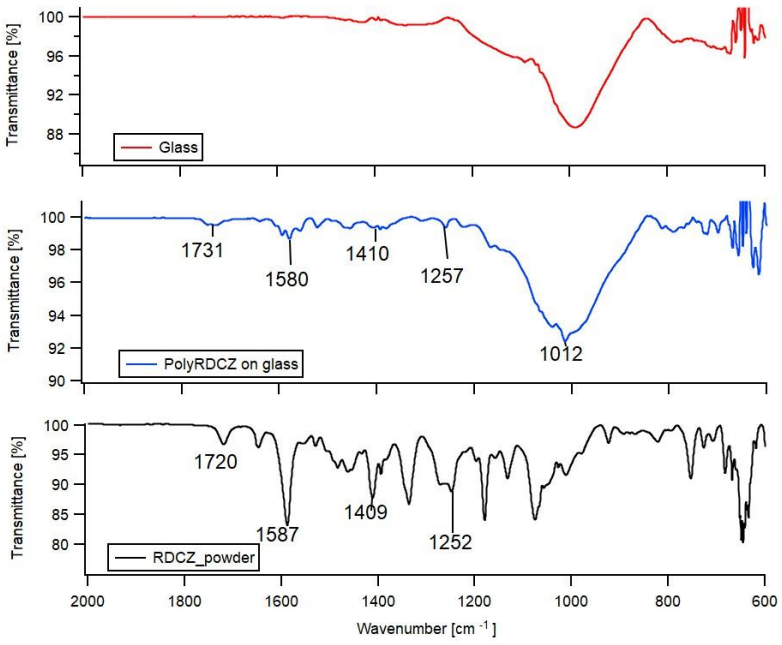

Figure 3.11 FTIR spectra of glass (top), PolyRDCZ on glass (middle), and RDCZ dyad (bottom). Sample for PolyRDCZ: Grid of dots 200x200 µm, thickness: 50 nm

The presence of the RDCZ moiety was confirmed by the appearance of peaks at 1731 cm^{-1} associated to the carbonyl group of RhB, and at 1580 cm^{-1} and 1410 cm^{-1} associated to the aromatic rings.[2]

Furthermore, this spectrum shows similar peaks to the PolyRDCZ prepared by electropolymerization (Figure 3.3) discussed previously. Nonetheless, in the photopolymerized case the broad 1012 cm^{-1} peak is attributed to the glass substrate; no characteristic doping peak is observed ~1125 cm^{-1} since no electrolyte was used in solution.

Then, the photophysical properties of the photopolymerized PolyRDCZ sample were investigated. To confirm the electrofluorochromic behavior of the polymer, a sample was prepared on ITO; a fluorescence image and spectra of PolyRDCZ is shown in Figure 3.12 (a and b).

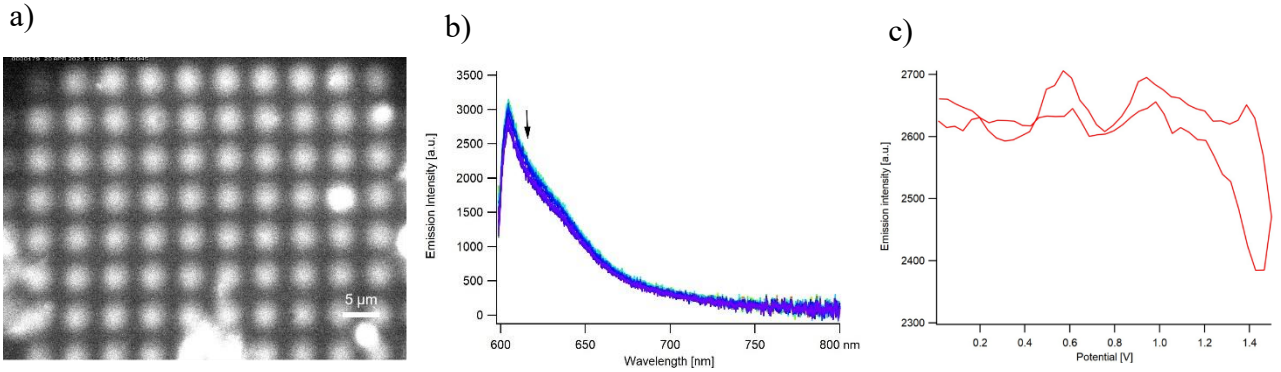

Figure 3.12 (a) Fluorescence image of PolyRDCZ on ITO. Exc: 561 nm. Exposure time: 600 ms (b) Emission spectra during oxidation from 0 V to 1.5 V, 0.1 V/s (c) Modulation of emission intensity at 610 nm during cyclic voltammetry.

A spectroelectrochemical experiment was conducted in the experimental set-up described previously in section 2.3 (Figure 2.1); using a three-electrode configuration and the ITO sample with the grafted PolyRDCZ as working electrode. The emission spectrum was recorded in-situ during a cyclic voltammetry experiment. The modulation observed (Figure 3.12c) confirms the electrofluorochromic behavior of the PolyRDCZ prepared by photopolymerization; which coincides with its electropolymerized counterpart (Figure 3.6c). Therefore, as in the electropolymerized PolyRDCZ, the fluorescence quenching on this system is due to the generation of a radical cation on the carbazole moiety by oxidation that quenches the emission from the rhodamine moeity.[3]

3.2.3 Micro/Nanofabrication by photopolymerization

The kinetics of the photopolymerization process is further investigated quantitatively by following the temporal evolution of the polymer optical volume density (OVD).[26, 28] As indicated in Fig.3.12, the kinetics of the photopolymerization process can be controlled both by limiting the exposure time and laser power.

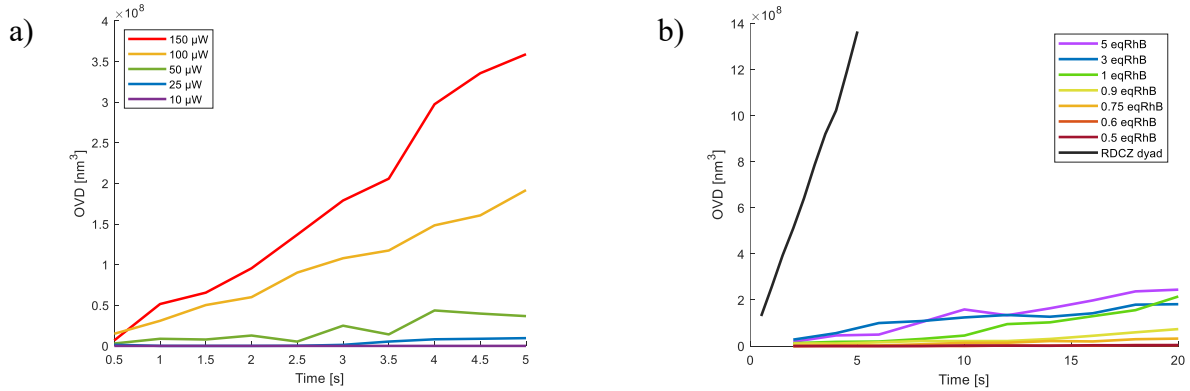

Figure 3.13 Evolution of OVD (Optical volume density) over time. (a) Power dependency of polymerization kinetics. (b) Effect of RhB concentration in the polymerization kinetics and comparison with RDCZ dyad. Samples: 0.01 M solution in DCE in a microcuvette (Height=10 µm) mounted on top of an inverted microscope. Magnification:100×1.5×2.5×. Substrate: Glass

In the case of the power dependency of the grafting kinetics, the laser power was systematically decreased until no photopolymerization was detectable at 10 µW (Figure 3.13a). The grafting rate was observed to increase linearly with increasing incident power.

The effect of the covalent bond in RDCZ was studied by comparing its grafting kinetics with separated RhB+CZ (Figure 3.13b) with increasing RhB/CZ rate. In the former case, the rate increases with the rhodamine concentration; until the concentration of carbazole becomes similar to the rhodamine. At this point, the rate becomes approximately constant since stoichiometry for the PET mechanism is 1:1. When compared to the separated RhB+CZ, the photopolymerization rates for the RDCZ dyad are observed to be substantially higher, which may be related to its better stability observed in Figure 3.9.

The better performance of the dyad system offers an advantage for the microfabrication of complex structures, therefore only this system will be considered for further studies. Using a piezo stage enables the obtention of complex forms, obtained by continuously scanning the sample position with the excitation laser, as detailed in section 2.5. This micro/nanofabrication approach is relatively fast (~ min) and does not require the use of a clean room.

This configuration was used to estimate the resolution and minimal thickness (Figure 3.14). The thickness was studied by grafting lines at increasing speed of the piezo stage, and the thickness limit observed is 5-10 nm. The lateral resolution is ~1 µm; circles of decreasing size were photografted until the smallest size where the center was still distinguishable was reached at r = 0.5 µm (Figure 3.14c). Nonetheless, since this process relays on optical methods, the resolution is fundamentally limited by the diffraction limit.[34]

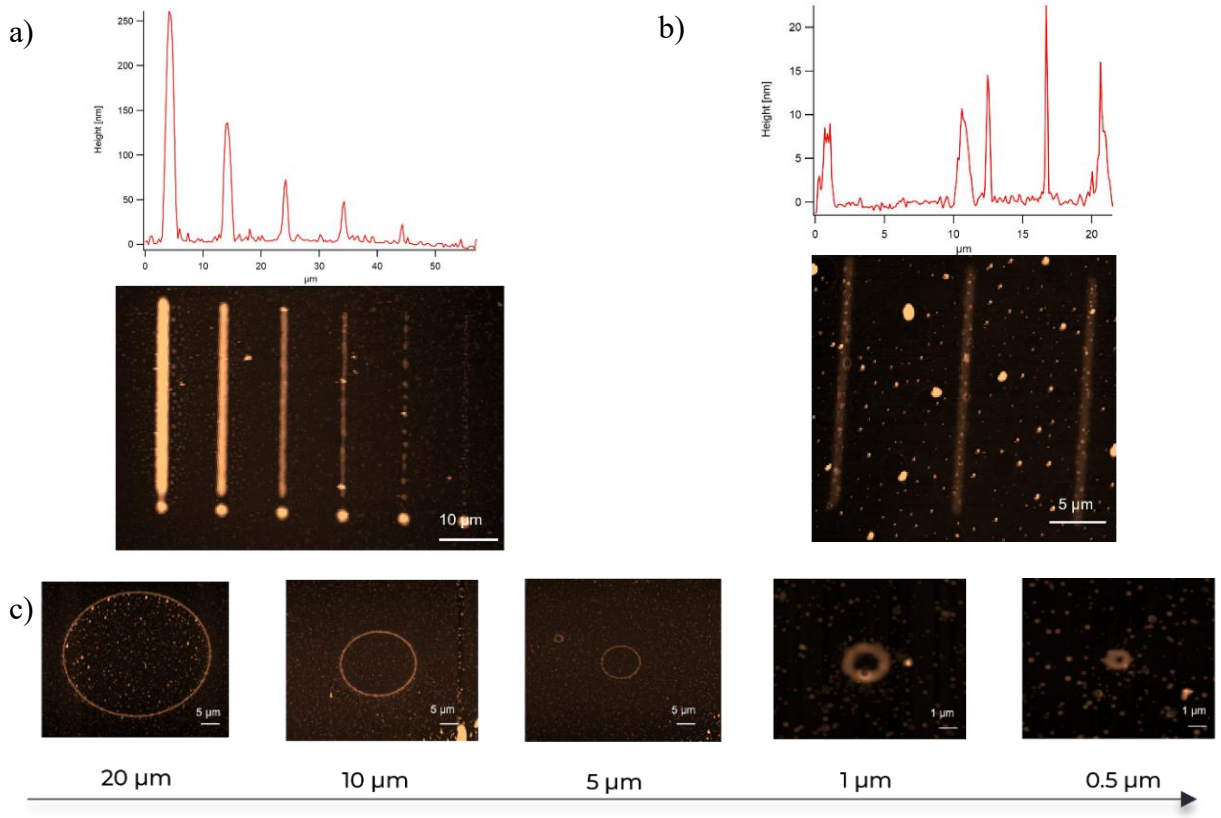

Figure 3.14 Thickness and resolution limits tests for structures constructed by photopolymerized PolyRDCZ. (a) Lines grafted at increasing speeds: 0.25, 0.5, 1, 2, 4, 8 µm/s. (b) Lines of 10 nm thickness. Speed: 4 µm/s. (c) Circles grafted with decreasing radius size. Power: 50 µW. Substrate: Glass.

3.3 Building of a molecular junction

3.3.1 Molecular junction between two gold electrodes and determination of conductivity

By definition, a molecular junction is a set-up consisting of one or more molecules connected between two electrodes.[7, 35] In this section we show that the local spatial control offered by the photopolymerization method allows the implementation of simple molecular junctions between two gold electrodes (micro/nanowire), using the experimental set-up described in section 2.5.

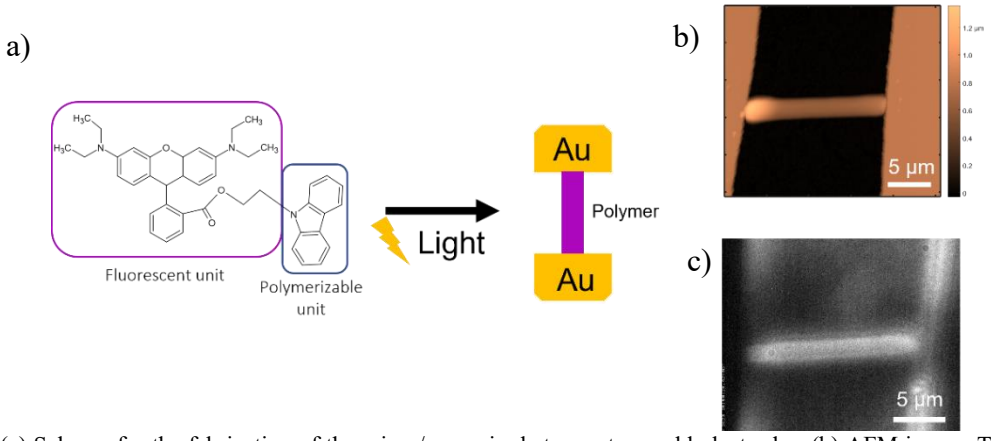

Figure 3.15 (a) Scheme for the fabrication of the micro/nanowire between two gold electrodes. (b) AFM image. The fabricated wires were ~ 3 µm wide (lateral), 15 µm long, and 0.6-1 µm thick (c) Fluorescence image. Exc: 560nm. Exposure time: 300 ms.

The wires were fabricated by continuously scanning the excitation laser (470 nm) between the two gold electrodes on a glass substrate, which was mounted on a cuvette containing a grafting solution (0.01M RDCZ + 10 % CZ). Figure 3.15 shows a general scheme of the fabrication, and an AFM and fluorescence image of a photografted junction.

This geometry readily allows for the determination of the conductivity of the PolyRDCZ nanowire. The two gold electrodes were connected to a potentiostat in a two-electrode configuration (working electrode and reference/counter electrode together). A potential bias was applied between the two gold electrodes in a cyclic voltammetry experiment without an electrolyte solution (dry state) to measure the conduction current. As expected for a resistive junction, the wire shows an ohmic behavior, where the current is directly proportional to the applied potential bias (Figure 3.16). This response was compared to the current measured with a blank (two gold electrodes not connected by the junction) and air (potentiostat not connected), both showing a flat response.

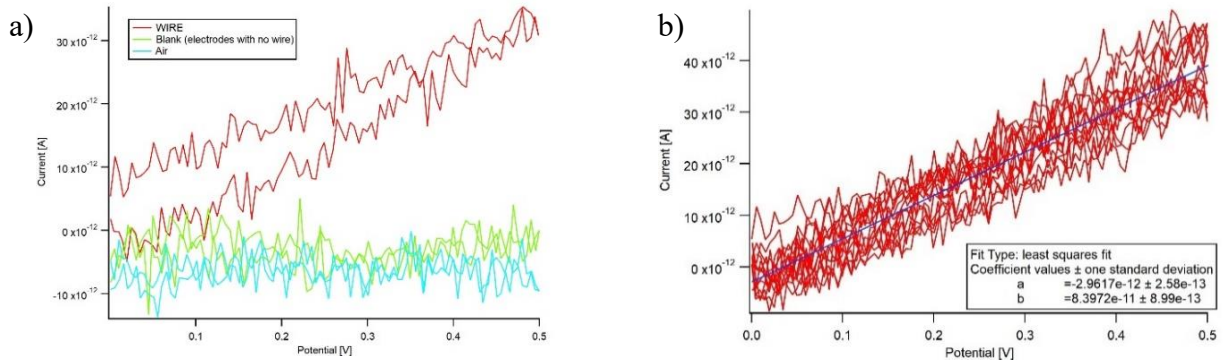

Figure 3.16 Cyclic voltammetry of micro/nanowire between two gold electrodes. 0 V to 0.5 V. (a) Comparison with blank (two gold electrodes not connected by the junction) and air (potentiostat not connected). (b) I vs V curve. 7 cycles. Increasing scan rate from 0.01 V/s to 0.5 V/s.

Then, the conductivity for each junction sample was determined by the slope of the I vs V curve (Figure 3.16b) and calculated as described in section 2.8. The average conductivity obtained for all samples was $(7.6\pm0.9)\times10^{-6}$ S cm^{-1}, which indicates that the PolyDRCZ behaves as a semiconductor.[36]

3.3.1 Molecular junction between a Pt ultramicroelectrode and a plasmonic substrate

The second PolyRDCZ molecular junction in this study, was fabricated vertically with a SECM coupled to an inverted microscope (experimental set-up described in section 2.3), as shown in Figure 3.17. In this geometry, different potentials can be applied to the two working electrodes (V_{tip} and V_{sub}) with respect to a reference electrode (Ag wire), generating a potential difference (V_{bias}).[4] The plasmonic excitation is generated by irradiation of the plasmonic substrate (ITO@AuNPs) with a focused red laser (650 nm). The current at the Pt UME tip (I_{tip}) corresponds to two different sources ($I_{tip}=I_{EC}+I_T$). The electrochemical current (I_{EC}) arises from the redox reaction of PolyRDCZ and RDCZ (in solution) at the tip. The transport current (I_T) is a current flowing between the Pt UME tip and the substrate due to the applied potential difference (V_{bias})[4] when both are connected; therefore, no influence of this current is expected when V_{bias}= 0 V ($V_{tip}=V_{sub}$). Furthermore, since PolyRDCZ has a low conductivity as previously demonstrated, the effect of I_T is expected to be less than I_{EC}.

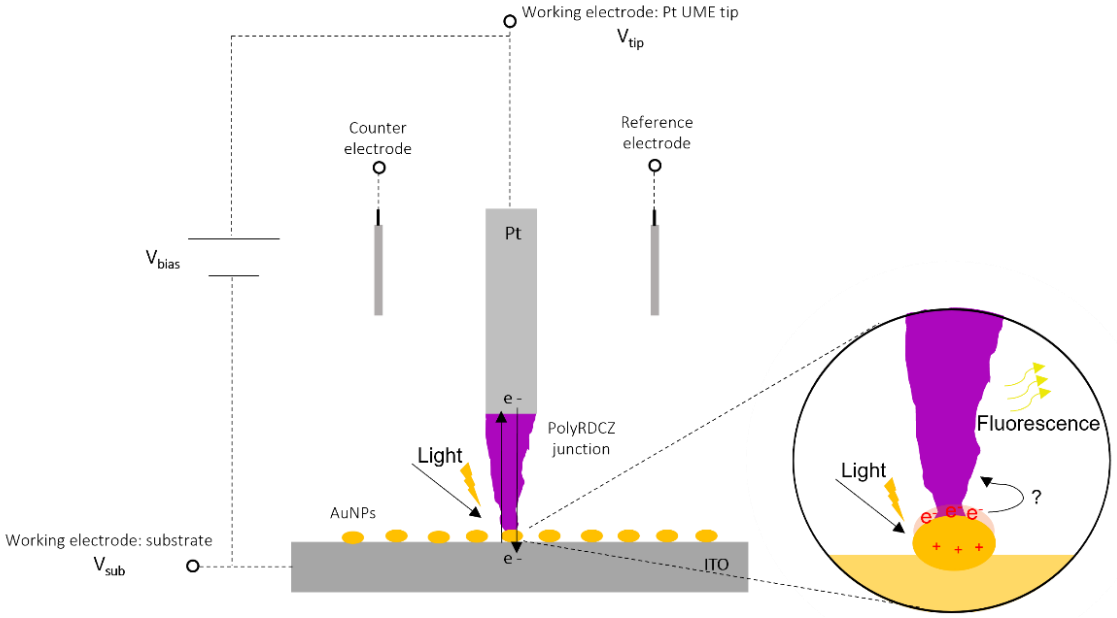

Figure 3.17 Molecular junction between a Pt UME tip and a plasmonic substrate (ITO@AuNPs). To study the junction, different potentials may be applied at the two working electrodes (V_{tip} and V_{sub}), generating a potential difference (V_{bias}). Simultaneously, the ITO@AuNPs may be irradiated with a 650 nm laser to excite the plasmon. The response is detected by electrical (current at Pt UME tip: I_{tip}) and optical methods (fluorescence).

The aim of studying this junction configuration is to observe the effect of plasmonic excitation on the conductivity of the conjugated polymer. This is possible by detecting the modulation on I_{tip} with the plasmon excitation since an increase in the current can be related to an increase in conductivity. Complementary to this, the use of an electrofluorochromic polymer like PolyRDCZ allows the use of fluorescence as an additional detection technique which is sensitive to phenomena induced by plasmon.[7, 24, 37] As was previously demonstrated, the fluorescence emission of this system is closely related to its redox state, switching from a neutral emissive state to an oxidated (more conductive) less emissive state.

The fabrication of molecular junctions with this configuration (which can be also considered as an electrochemical transistor) was previously reported for conductive polymers like PEDOT[4] and PANI[21] using a purely electropolymerization approach. This protocol proved to be unsuccessful for the

PolyRDCZ system due to its low conductivity (7.6×10^{-6} S cm^{-1} compared to 200 S cm^{-1} for PEDOT and 100 S cm^{-1} for PANI) impeding the achievement of sufficiently thick films to fill the gap between the tip and the substrate.

Nonetheless, the photo- and electropolymerization capacity of RDCZ proved to be the answer to create a successful procedure for the junction fabrication. Figure 3.18 shows a scheme of the photo/electrochemical protocol used; all the fabrication was performed on a cuvette filled with a 0.01 M RDCZ+10%CZ solution mounted on the experimental set-up in Figure 2.1.

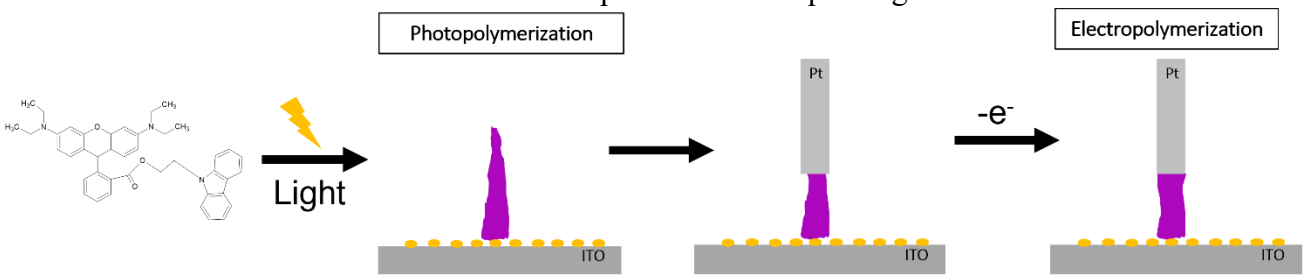

Figure 3.18 Scheme of the photo/Electrochemical protocol to fabricate the molecular junction.

First, a PolyRDCZ column (15-20 µm) was prepared by photopolymerization using a 470 nm laser focused on the ITO@AuNPs substrate. Then, the Pt UME tip was approached and pressed on the PolyRDCZ column until a 10 µm distance from the substrate was reached. Finally, the connection between the tip and the PolyRDCZ column was completed by performing electropolymerization on the tip by cyclic voltammetry for ~40 cycles. The purpose of this procedure is to ensure the best possible connection between the tip and the grafted PolyRDCZ and thus between tip and substrate.

Since this is a novel approach for the fabrication of this system, some additional precautions were taken: (1) the polymerization was followed optically at the tip (2) the electropolymerization was continued until the CV response was stable (3) different V_{bias} were applied to test the junction before plasmonic experiments (4) the junction was purposely broken at the end of the experiment and tested for comparison.

To test the plasmon effect on the PolyRDCZ molecular junction, the ITO@AuNPs substrate was excited using a 650 nm laser, which matches its plasmonic excitation band (Figure 2.3b). For this experiment, different V_{sub} were applied with a constant V_{tip}= 1 V to observe the effect of V_{bias} on the junction response. Simultaneously ON/OFF cycles of the plasmonic excitation were applied as shown in Figure 3.19. It can be noted that I_{tip} increases when a non-zero V_{bias} is applied, this can be attributed to a transport current passing through the junction[38] as well as an increased positive feedback current from the RDCZ solution.[18]

The PolyRDCZ junction showed an increase in I_{tip} and a decrease in emission intensity (Figure 3.19a), which suggests a possible oxidation of the system in accordance with the previous electrofluorochromic characterization (Figure 3.6). An opposite effect has been previously reported for a PEDOT junction, where the plasmons were found to reduce the polymer from oxidized to neutral state due to hot electrons injections generated by LSPR.[4]

Since the PolyRDCZ tests were performed in presence of the precursor RDCZ solution, the experiment was repeated without the grafted junction (Figure 3.19b) for comparison. I_{tip} shows an increase with laser irradiation, however with a much smaller amplitude in comparison to the junction case. This could be attributed to a local temperature increase due to thermal dissipation in the metal nanoparticles[22] or local heating due to the laser. Furthermore, no fluorescence quenching is observed

in absence of the junction; instead, there is a small increase in the emission intensity attributed to scattering of the irradiation laser.

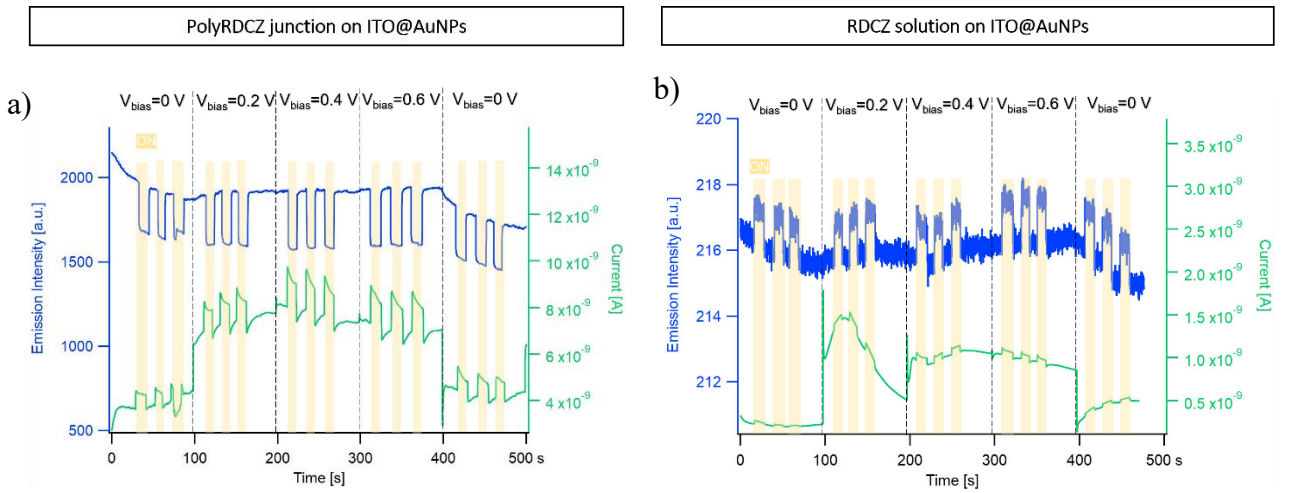

Figure 3.19 Modulation of the current at the Pt UME tip I_{tip} (green) and emission intensity (blue) with ON/OFF cycles of plasmonic excitation for (a) a PolyRDCZ junction (10 µm) between the Pt UME tip and the ITO@AuNPs substrate and (b) a 0.01M RDCZ+10%CZ solution in DCM+0.1M $TBAPF_6$ with the Pt UME tip at 10 µm from the ITO@AuNPs substrate. Potentials applied: V_{tip}: 1 V (constant) and V_{sub}=1 V, 0.8 V, 0.6 V, 0.4 V, 1 V with a 100 s step.

The effect of the PolyRDCZ system was further tested by purposely breaking the junction. I_{tip} and emission intensity modulation of the intact and broken junction are shown in Figure 3.20.

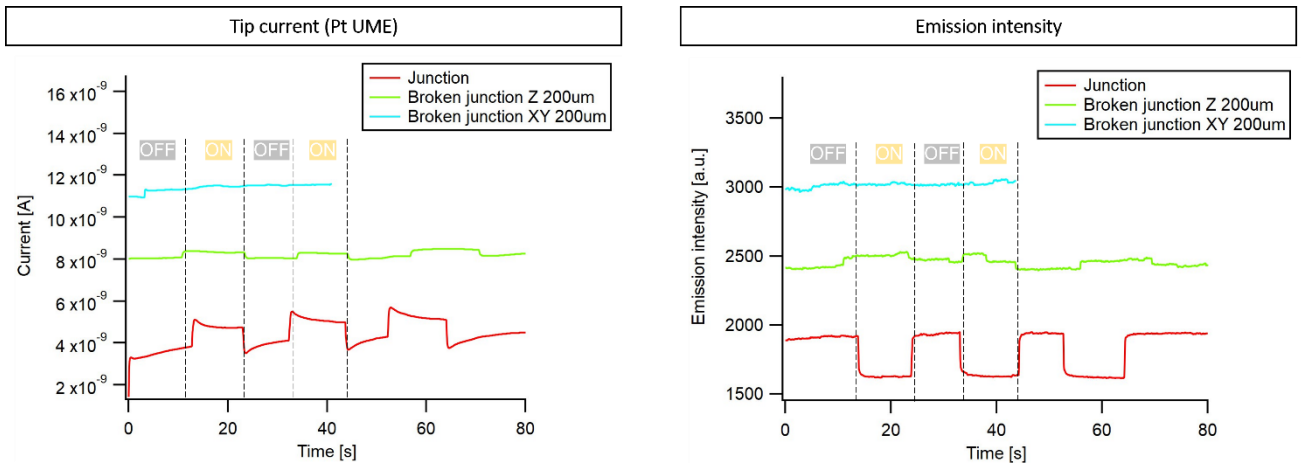

Figure 3.20 Effect of breaking the PolyRDCZ junction. Modulation of the current I_{tip} and emission intensity with ON/OFF cycles of plasmonic excitation before (red) and after breaking the junction by moving 200 µm up in Z-axis (green) and 200 µm horizontally in XY-axis (cyan). V_{tip}=1 V. V_{sub}=0.8 V (V_{bias}=0.2 V). All experiments were conducted in presence of a 0.01 M RDCZ + 10 % CZ solution in DCM+0.1 M $TBAPF_6$. An offset was added to current and emission curves for clearer visualization.

First, the Pt UME tip was moved 200 µm up in Z-axis. The I_{tip} modulation decreased dramatically far from the substrate, and no fluorescence quenching was observed. Then, the tip was moved back to its original position in the Z-axis (10 µm) and moved 200 µm horizontally in XY-axis. As expected, no modulation (I_{tip} or fluorescence) was observed with plasmon excitation since the tip was no longer aligned with the irradiation laser. These results indicate that the coupled I_{tip} increase with fluorescence quenching is actually related to the presence of the molecular junction.

To elucidate the plasmon effect exerted by the AuNPs on the PolyRDCZ junction from other phenomena induced by the light irradiation or the ITO conductive substrate, a similar junction was grafted on bare ITO. The modulation of I_{tip} and emission in the two junctions was compared with V_{tip}= 1.5 V and V_{sub}= 1.5 V or 0.7 V (Figure 3.21).

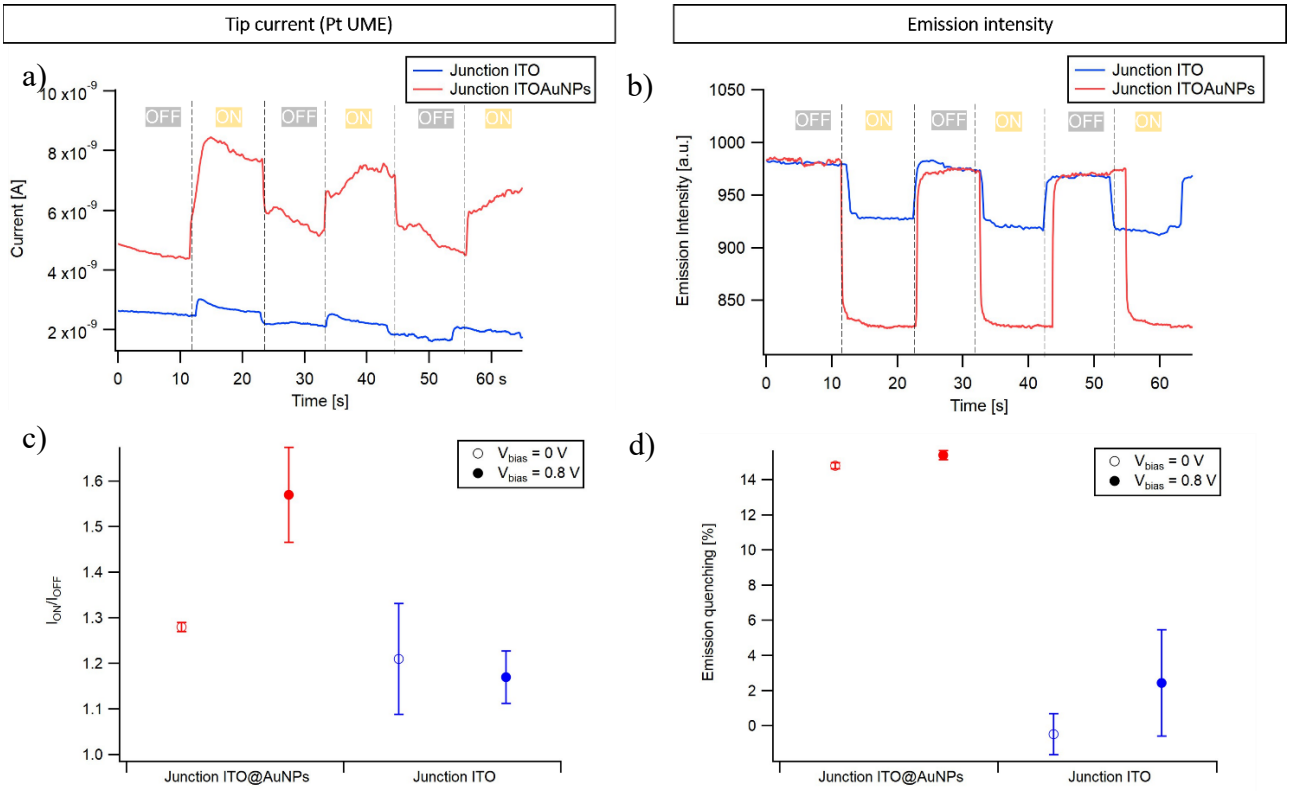

Figure 3.21 Comparison of PolyRDCZ junction on ITO@AuNPs and ITO. [Top] (a) Itip and (b) emission intensity modulation with ON/OFF cycles of 650 nm laser irradiation. V_{tip}= 1.5 V. V_{sub}= 1.5 V (V_{bias}= 0 V). [Bottom] (c) ION/IOFF ratio and (d) emission quenching comparison for identical experiments with V_{bias}= 0 V (V_{tip}= 1.5 V. V_{sub}= 1.5 V) and V_{bias}= 0.8 V .(V_{tip}= 1.5 V. V_{sub}= 0.7 V). All experiments were conducted in presence of a 0.01 M RDCZ + 10 % CZ solution in DCM+0.1 M $TBAPF_6$. An offset was added to current and emission curves for clearer comparison.

Both the modulation in I_{tip} and in emission intensity are clearly diminished in the case of a junction grafted on bare ITO. Therefore, the LSPR on AuNPs interacts with the PolyRDCZ junction to generate the increase in I_{tip} (higher I_{ON}/I_{OFF} ratio) and fluorescence quenching (higher emission quenching %). Even if these results indicate an LSPR induced oxidation of the PolyRDCZ junction due to injection of hot charge carriers in the vicinity of the AuNPs[4], other plasmon-induced effects should also be considered, among which thermal effects and local electric field enhancement.

Fluorescence is known to be sensitive to the electric field enhancement generated by LSPR.[39] Also, highly efficient quenching has been reported due to energy transfer between the fluorophore and metallic nanoparticle.[24] In this system, the emission spectrum of PolyRDCZ (Figure 3.6c) is clearly overlapped with the absorption spectrum of the ITO@AuNPs substrate (Figure 2.3b); therefore, the former case is a possible scenario.

Another interesting observation to be noted is that fluorescence quenching appears only in experiments with a grafted junction, but not in solution or with a broken junction (Figure 3.19 & Figure 3.20) despite the presence of emissive RD in solution. Additionally, the I_{ON}/I_{OFF} ratio seems to be enhanced with a non-zero V_{bias} particularly for the junction on ITO@AuNPs (Figure 3.21c), while the emission quenching is less affected.

The effect observed in absence of AuNPs suggests a contribution purely from the light irradiation, either a photoinduced effect[40] due to absorbance of the PolyRDCZ system or a thermal effect due to local heating caused by the laser.

These results indicate that the effect observed on the PolyRDCZ junction on ITO@AuNPs arises from the collective effect of complex interactions and further studies are required. The complexity of the fabrication protocol for this junction originates structural differences in the junctions prepared limiting the reproducibility. For this reason, the optimization of this protocol is required to further investigate the influence of other variables during the plasmonic excitation tests. For example, AuNPs of different sizes could be tested to reduce the spectral overlap with RDCZ and elucidate the effect of energy transfer. Also, to confirm the effect of light irradiation in absence of AuNPs the experiment could be repeated with variations in the laser power.

4. Conclusions and future perspectives

The polymerization of the EFC system RDCZ was explored by both electrochemical and photophysical methods to obtain the PolyRDCZ conjugated polymer. The electropolymerization of this molecule was achieved by CV or CA, as previously reported for other carbazole derivatives. Nonetheless, in the case of RDCZ this procedure proved to require the use of high concentrations and addition of a small amount of pure CZ, presumably due to steric hinderance constrains.

The photopolymerization of RDCZ was found to be possible due to the photoinduced electron transfer (PET) from the excited rhodamine moiety to the carbazole to produce the carbazyl cationic radical which triggers the polymerization. This methodology allows for micro/nanofabrication through direct laser writing with high spatial resolution and thickness limits up to 5-10 nm.

PolyRDCZ produced by either of the previous methods showed promising electrofluorochromic properties, the conjugated polymer being able to be switched from its neutral state to an oxidized less fluorescent state at 1.5 V. A photopolymerized PolyRDCZ wire between two gold electrodes was used to determine its conductivity as $(7.6\pm0.9)\times10^{-6}$ S cm^{-1}, locating the material in the semiconductor range.

The photo- and electropolymerization capacity of RDCZ allowed to create a successful procedure for the fabrication of a molecular junction between a Pt ultramicroelectrode and a plasmonic substrate. A coupled response of current increase and fluorescence quenching was observed due to plasmon-induced effects in the PolyRDCZ junction. Nonetheless, the response seems to arise from the collective effect of complex interactions. Further research on this system and the effect of different variables involved (NP size, laser power, junction size, etc.) could lead to possible fine tuning of redox and fluorescent properties through electrochemical or light excitation. This field of study is relevant for the future development of multimodal molecular electronic devices with applications as displays, sensors, and optoelectronic devices.

5. Acknowledgements

None of this work would have been possible without the support of my supervisors Pr. Fabien Miomandre and Dr. Vitor Brasiliense. Thanks a lot for the guidance, the discussions, and experiment ideas which really pushed forward my professional development along with the project. I would also like to extend a big appreciation to Jeff Audibert, for all the support and training with all the different optical experiments. Thank you also to Baptiste Maillot and Ali Dabbous for all the support during my internship. And thank you to all the rest of the people at PPSM for being so helpful whenever I needed.

I would also like to thank the Erasmus Mundus SERP+ master program and the European Commission for financing my scholarship for the past two years, and for the opportunity to study in such an enriching and international environment.

6. References

(1) Audebert, P.; Miomandre, F. Electrofluorochromism: from molecular systems to set-up and display. *Chem. Sci.* **2013**, *4* (2), 575-584. DOI: 10.1039/c2sc21503a.
(2) Ayranci, R.; Demirkol, D. O.; Timur, S.; Ak, M. Rhodamine-based conjugated polymers: potentiometric, colorimetric and voltammetric sensing of mercury ions in aqueous medium. *Analyst* **2017**, *142* (18), 3407-3415. DOI: 10.1039/c7an00606c.
(3) Miomandre, F.; Audebert, P. *Luminescence in Electrochemistry. Applications in Analytical Chemistry, Physics and Biology*; Springer, 2017.
(4) Ai, Y.; Nguyen, V. Q.; Ghilane, J.; Lacaze, P. C.; Lacroix, J. C. Plasmon-Induced Conductance Switching of an Electroactive Conjugated Polymer Nanojunction. *ACS Appl Mater Interfaces* **2017**, *9* (33), 27817-27824. DOI: 10.1021/acsami.7b04695.
(5) Corrente, G. A.; Beneduci, A. Overview on the Recent Progress on Electrofluorochromic Materials and Devices: A Critical Synopsis. *Adv. Optical Mater.* **2020**, 2000887. DOI: 10.1002/adom.202000887
(6) Miomandre, F. How molecular electrochemistry may shine light by designing electrofluorochromic compounds. *Current Opinion in Electrochemistry* **2020**. DOI: 10.1016/j.coelec.2020.07.003.
(7) Wang, M.; Wang, T.; Ojambati, O. S.; Duffin, T. J.; Kang, K.; Lee, T.; Scheer, E.; Xiang, D.; Nijhuis, C. A. Plasmonic phenomena in molecular junctions: principles and applications. *Nat Rev Chem* **2022**, *6* (10), 681-704. DOI: 10.1038/s41570-022-00423-4.
(8) Hoffmann, M.; Schletz, D.; Steiner, A. M.; Wolf, D.; Mayer, M.; Fery, A. Conjugated Polymer–Gold–Silver Hybrid Nanoparticles for Plasmonic Energy Focusing. *The Journal of Physical Chemistry C* **2022**, *126* (5), 2475-2481. DOI: 10.1021/acs.jpcc.1c08583.
(9) Ates, M.; Uludag, N. Carbazole derivative synthesis and their electropolymerization. *Journal of Solid State Electrochemistry* **2016**, *20* (10), 2599-2612. DOI: 10.1007/s10008-016-3269-5.
(10) Karon, K.; Lapkowski, M. Carbazole electrochemistry: a short review. *Journal of Solid State Electrochemistry* **2015**, *19* (9), 2601-2610. DOI: 10.1007/s10008-015-2973-x.
(11) Ambrose, J. F.; Nelson, R. F. Anodic Oxidation Pathways of Carbazoles. *Journal of The Electrochemical Society* **1968**, *115* (11). DOI: 10.1149/1.2410929.
(12) Contal, E.; Sougueh, C. M.; Lakard, S.; Et Taouil, A.; Magnenet, C.; Lakard, B. Investigation of Polycarbazoles Thin Films Prepared by Electrochemical Oxidation of Synthesized Carbazole Derivatives. *Frontiers in Materials* **2019**, *6*. DOI: 10.3389/fmats.2019.00131.
(13) Diaz, A. F.; Kanazawa, K. K.; Gardini, G. P. Electrochemical polymerization of pyrrole. *Journal of the Chemical Society, Chemical Communications* **1979**, (14). DOI: 10.1039/c39790000635.
(14) Cosnier, S.; Karyakin, A. *Electropolymerization. Concepts, Materials and Applications*; Wiley-VCH, 2010.
(15) Yagci, Y.; Jockusch, S.; Turro, N. J. Photoinitiated Polymerization: Advances, Challenges, and Opportunities. *Macromolecules* **2010**, *43* (15), 6245-6260. DOI: 10.1021/ma1007545.
(16) Pan, X.; Tasdelen, M. A.; Laun, J.; Junkers, T.; Yagci, Y.; Matyjaszewski, K. Photomediated controlled radical polymerization. *Progress in Polymer Science* **2016**, *62*, 73-125. DOI: 10.1016/j.progpolymsci.2016.06.005.
(17) Li, M.; Cushing, S. K.; Wu, N. Plasmon-enhanced optical sensors: a review. *Analyst* **2015**, *140* (2), 386-406. DOI: 10.1039/c4an01079e.
(18) Bard, A. J.; Faulkner, L. R. *ELECTROCHEMICAL METHODS Fundamentals and Applications*; John Wiley & Sons, Inc, 2001.
(19) Guerret-Legras, L.; Audibert, J. F.; Dubacheva, G. V.; Miomandre, F. Combined scanning electrochemical and fluorescence microscopies using a tetrazine as a single redox and luminescent (electrofluorochromic) probe. *Chem Sci* **2018**, *9* (27), 5897-5905. DOI: 10.1039/c8sc01814f.
(20) Janin, M.; Ghilane, J.; Lacroix, J.-C. Scanning electrochemical microscopy for the fabrication of copper nanowires: Atomic contacts with quantized conductance, and molecular adsorption effect. *Electrochimica Acta* **2012**, *83*, 7-12. DOI: 10.1016/j.electacta.2012.07.115.
(21) Janin, M.; Ghilane, J.; Randriamahazaka, H.; Lacroix, J. C. Electrochemical fabrication of highly stable redox-active nanojunctions. *Anal Chem* **2011**, *83* (24), 9709-9714. DOI: 10.1021/ac202788y.
(22) Kim, M.; Lee, J. H.; Nam, J. M. Plasmonic Photothermal Nanoparticles for Biomedical Applications. *Adv Sci (Weinh)* **2019**, *6* (17), 1900471. DOI: 10.1002/advs.201900471.
(23) Su, Q.; Jiang, C.; Gou, D.; Long, Y. Surface Plasmon-Assisted Fluorescence Enhancing and Quenching: From Theory to Application. *ACS Appl Bio Mater* **2021**, *4* (6), 4684-4705. DOI: 10.1021/acsabm.1c00320.

(24) Fan, C.; Wang, S.; Hong, J. W.; Bazan, G. C.; Plaxco, K. W.; Heeger, A. J. Beyond superquenching: hyper-efficient energy transfer from conjugated polymers to gold nanoparticles. *Proc Natl Acad Sci U S A* **2003**, *100* (11), 6297-6301. DOI: 10.1073/pnas.1132025100.
(25) Eaton, D. F. Recommended methods for fluorescence decay analysis. *Pure and Applied Chemistry* **1990**, *62* (8), 1631-1648. DOI: 10.1351/pac199062081631.
(26) Brasiliense, V.; Audibert, J. F.; Wu, T.; Tessier, G.; Berto, P.; Miomandre, F. Local Surface Chemistry Dynamically Monitored by Quantitative Phase Microscopy. *Small Methods* **2022**, *6* (1), e2100737. DOI: 10.1002/smtd.202100737.
(27) Berto, P.; Rigneault, H.; Guillon, M. Wavefront sensing with a thin diffuser. *Opt Lett* **2017**, *42* (24), 5117-5120. DOI: 10.1364/OL.42.005117.
(28) Maillot, B.; Johnson, M.; Audibert, J. F.; Miomandre, F.; Brasiliense, V. Operando surface optical nanometrology reveals diazonium salts' visible photografting mechanism. *Nanoscale* **2023**. DOI: 10.1039/d3nr00439b.
(29) Data, P.; Zassowski, P.; Lapkowski, M.; Domagala, W.; Krompiec, S.; Flak, T.; Penkala, M.; Swist, A.; Soloducho, J.; Danikiewicz, W. Electrochemical and spectroelectrochemical comparison of alternated monomers and their copolymers based on carbazole and thiophene derivatives. *Electrochimica Acta* **2014**, *122*, 118-129. DOI: 10.1016/j.electacta.2013.11.167.
(30) Soganci, T.; Baygu, Y.; Gök, Y.; Ak, M. Disulfide-linked symmetric N-alkyl carbazole derivative as a new electroactive monomer for electrochromic applications. *Synthetic Metals* **2018**, *244*, 120-127. DOI: 10.1016/j.synthmet.2018.07.009.
(31) Peerce;, P. J.; Bard, A. J. Polymer films on electrodes: Part III. Digital simulation model for cyclic voltammetry of electroactive polymer film and electrochemistry of poly(vinylferrocene) on platinum. *J. Electroanal Chem.* **1980**, *114* (1), 89-115. DOI: 10.1016/s0022-0728(80)80438-4
(32) Fischer, A. B.; Bronstein-Bonte, I. Photoinduced electron transfer quenching of rhodamine B in polymer films. *Journal of Photochemistry* **1985**, *30* (4), 475-485. DOI: 10.1016/0047-2670(85)85064-4.
(33) Valeur, B. *Molecular Fluorescence Principles and Applications*; WILEY-VCH, 2002.
(34) Bagheri, A.; Jin, J. Photopolymerization in 3D Printing. *ACS Applied Polymer Materials* **2019**, *1* (4), 593-611. DOI: 10.1021/acsapm.8b00165.
(35) Li, T.; Bandari, V. K.; Schmidt, O. G. Molecular Electronics: Creating and Bridging Molecular Junctions and Promoting Its Commercialization. *Adv Mater* **2023**, *35* (22), e2209088. DOI: 10.1002/adma.202209088.
(36) Kaur G., A. R., Cass P., Bown M., Gunatillake P. Electrically conductive polymers and composites for biomedical applications. *RSC Advances* **2015**, *5*, 37553-37567. DOI: 10.1039/C5RA01851J
(37) Lakowicz, J. R.; Ray, K.; Chowdhury, M.; Szmacinski, H.; Fu, Y.; Zhang, J.; Nowaczyk, K. Plasmon-controlled fluorescence: a new paradigm in fluorescence spectroscopy. *Analyst* **2008**, *133* (10), 1308-1346. DOI: 10.1039/b802918k.
(38) Friedlein, J. T.; McLeod, R. R.; Rivnay, J. Device physics of organic electrochemical transistors. *Organic Electronics* **2018**, *63*, 398-414. DOI: 10.1016/j.orgel.2018.09.010.
(39) Kang, K. A.; Wang, J.; Jasinski, J. B.; Achilefu, S. Fluorescence manipulation by gold nanoparticles: from complete quenching to extensive enhancement. *J Nanobiotechnology* **2011**, *9*, 16. DOI: 10.1186/1477-3155-9-16.
(40) Furmansky, Y.; Sergani, S.; Ashkenasy, N.; Visoly-Fisher, I. Photoconductance of ITO/Conductive Polymer Junctions in the UV and Visible Ranges. *The Journal of Physical Chemistry C* **2018**, *122* (13), 7288-7295. DOI: 10.1021/acs.jpcc.8b00826.